Construction and Building Materials 510 (2026) 145234

Contents lists available at ScienceDirect

Construction and Building Materials

journal homepage: www.elsevier.com/locate/conbuildmat

Experimental investigation of nonlinear stress-strain behaviour of various elastomeric materials under cyclic loading

Hailong Cao [a,*], Karl Minta [a], Hossein A. Beigi [a], Evangelia Georgantzia [b], Mohammad M. Kashani [a]

[a] School of Engineering, Faculty of Engineering and Physical Sciences, University of Southampton, Southampton SO16 7QF, United Kingdom
[b] School of Civil, Aerospace and Design Engineering, Faculty of Science and Engineering, University of Bristol, Bristol, BS8 1TR, United Kingdom

ARTICLE INFO

Keywords:
Cyclic tests
Nonlinear response
Energy dissipation
Residual deformation
Creep
Elastomeric material

ABSTRACT

This study investigates the nonlinear mechanical responses of elastomeric materials under complex loading paths. The experimental programme involved a series of uniaxial tensile and compressive tests under various loading protocols, systematically comparing the mechanical responses of different materials. The results show that amorphous polymers, including Thermoplastic Polyurethane, Neoprene rubber, and Neoprene/NBR rubber, exhibit more linear (elastic) load–unload behaviour, with improved shape recovery, resistance to stress relaxation, and reduced residual strain, although their energy dissipation capacity remains limited. In contrast, semi-crystalline polymers, including Polypropylene, Ultra-High-Molecular-Weight Polyethylene, and High-Density Polyethylene, demonstrate pronounced strain-dependent behaviour. As the strain increases, stress softening and cyclic relaxation effects are reduced. These materials exhibit significant energy dissipation but considerable residual strain. A key outcome of this research is that Thermoplastic Polyurethane presents the most favourable combination of high stress retention, low residual strain, and creep resistance, making it a strong candidate for use in the segmental construction of prefabricated bridges as a seismic damage-avoidance element. Ultra-High-Molecular-Weight Polyethylene, when combined with post-tension systems, also shows potential due to its strain hardening and enhanced energy dissipation, thereby improving seismic resilience under major events. These findings provide valuable insights into the deformation mechanisms of elastomeric materials and offer practical guidance for their effective implementation in energy-dissipating structural systems.

1. Introduction

Concrete bridges are critical nodes in modern transportation infrastructure networks. At present, many bridges are suffering from corrosion and material degradation. Long-term ageing and reinforcement corrosion have led to a reduction in both the residual load-bearing capacity and ductility of these structures [1–4], making them more vulnerable to seismic events. Modern seismic design practices emphasise ductility, whereby bridge piers are expected to undergo controlled damage in potential plastic hinge regions to dissipate seismic energy [5–10]. However, this often renders piers unserviceable after large earthquakes, mainly due to excessive residual deformations. For instance, following the 1995 Kobe earthquake, over 100 reinforced concrete columns with excessive residual displacements had to be demolished [11]. It is an indication of the lack of resilience in the design approach adopted by transport sector. There is therefore an urgent need to replace vulnerable bridges and to develop a new generation of innovative and resilient structures that can withstand both material deterioration and seismic hazards.

Previous studies have shown that precast post-tensioned segmental (PPS) bridge piers, developed within Accelerated Bridge Construction (ABC) concept, are an excellent alternative to conventional bridge structures due to their rapid construction and potential for post-earthquake repairability [12–22]. However, two shortcomings cannot be overlooked: (i) additional energy-dissipating components are required to provide sufficient damping to meet seismic demands; and (ii) severe concrete damage has been observed in the high contact-stress regions between adjacent precast segments. To prevent permanent damage caused by irreversible plastic deformation of structural columns after earthquakes, Kashani et al. [23–25] proposed a biomechanically

* Corresponding author.
E-mail addresses: hc14n23@soton.ac.uk (H. Cao), km5g22@soton.ac.uk (K. Minta), aghabeigi@soton.ac.uk (H.A. Beigi), evangelia.georgantzia@bristol.ac.uk (E. Georgantzia), mehdi.kashani@soton.ac.uk (M.M. Kashani).

https://doi.org/10.1016/j.conbuildmat.2026.145234
Received 10 November 2025; Received in revised form 24 December 2025; Accepted 10 January 2026
Available online 15 January 2026

inspired damage-free pier system inspired from the human spine, as illustrated in Fig. 1. In this system, specific flexible materials are used to replicate the function of intervertebral discs, which not only provide flexibility but also effectively absorb and dissipate external forces, thereby preventing permanent damage to the concrete segments (analogous to vertebrae). However, studies have shown that conventional rubber layers are unable to provide sufficient energy dissipation, while the subsequently tested entangled wire materials exhibit significant deformation due to its low stiffness [23,24]. These findings highlight the need to develop a material with both high energy dissipation capacity and sufficient stiffness to serve as an ideal intervertebral disc analogue.

In this study, six polymeric materials commonly used in engineering applications were investigated, including Thermoplastic Polyurethane (TPU), Neoprene rubber, Neoprene/NBR rubber, Polypropylene (PP), Ultra-High-Molecular-Weight Polyethylene (UHMWPE), and High-Density Polyethylene (HDPE). Rubber material, as a highly elastic material, is one of the earliest developed and most mature isolation materials, widely used in critical structures such as buildings, bridges, and has also been investigated for application in nuclear power plants [26–28]. Compared to conventional rubber material, polyurethane offers superior load-bearing capacity and energy dissipation, and has been explored as a promising alternative to high-damping rubber in seismic engineering [19,29,30]. As semi-crystalline materials, plastics have been widely used in the aerospace, electrical, and construction industries owing to their low density, high specific strength, and excellent formability [31]. Among them, polyethylene and polypropylene occupy an important position in the plastics industry due to their low cost and satisfactory performance. These advantageous characteristics make the above materials promising candidates for use as “intervertebral disc” (IRD) components in damage-free and self-centring spinal-column bridge piers.

It is worth noting that the mechanical responses of the aforementioned elastomeric materials exhibit pronounced nonlinearity, characterised by stress softening, relaxation, time dependency, and strong hysteresis. These macroscopic physical behaviours are governed by their distinctive microstructural features [32,33]. In previous studies, numerous constitutive models have been developed to characterise the mechanical responses of amorphous polymers (such as rubber and polyurethane) and semi-crystalline polymers (such as polypropylene and polyethylene) under experimental conditions [30,34–38]. However, most of these models are limited to simple monotonic or basic cyclic loading conditions [39–41]. Constitutive models calibrated under simple loading protocols often perform poorly when validated against complex loading paths that activate multiple nonlinear mechanisms simultaneously. These models generally struggle to capture all nonlinear behaviours such as hysteresis, stress softening and rate-dependent responses [42,43] and often fail to provide meaningful insight into more complex deformation responses. Recently, Reyes et al. [44] demonstrated that, with appropriate calibration, certain models are capable of capturing path relaxation phenomena observed in experiments, offering new perspectives on the deformation mechanisms of materials under complex loading. Models calibrated using protocols that simultaneously trigger multiple response mechanisms may possess the ability to simulate and predict various structural behaviours independently in subsequent analyses. More recently, a number of studies have used hybrid modelling approaches, such as the Parallel Rheological Framework, to characterise the complex mechanical behaviour of materials under a wide range of conditions [44–46].

While the mechanical properties of these materials, particularly rubbers, have been investigated in previous studies [28,35,36,39,41,42], there remains very limited experimental evidence [19,29,30] and fundamental data assessing their potential application in segmental bridge construction. In this paper, we address this research gap by conducting comprehensive cyclic tension and compression tests on six polymeric materials, considering the influence of large strain levels, repeated cyclic loading, and complex strain conditions on flow stress, energy dissipation capacity, stiffness, and residual deformation. The results provide essential insights for identifying suitable candidates to be used as energy dissipation interlayers in damage free segmental bridge piers.

2. Experimental campaign

To characterise the mechanical behaviour of the six elastomeric materials, a total of 66 material tests were conducted, including 30 tensile tests (comprising five loading cycles for each of six specimens) and 36 compression tests (comprising six loading cycles for each of six specimens) described in the following sections.

2.1. Specimen specification

In this study, six elastomeric materials (TPU, Neoprene, Neoprene/NBR, UHMWPE, PP, and HDPE) were tested, all sourced from UK manufacturers, with their mechanical properties summarised in Table 1. Compression set refers to the residual deformation after compression and recovery. Tensile and compressive specimens were prepared by cutting from rectangular raw material sheets. All specimens were prepared using a waterjet cutting machine at the Engineering Design and Manufacturing Centre (EDMC) workshop at the University of Southampton. Fig. 2 shows the geometry of the dumbbell-shaped tensile

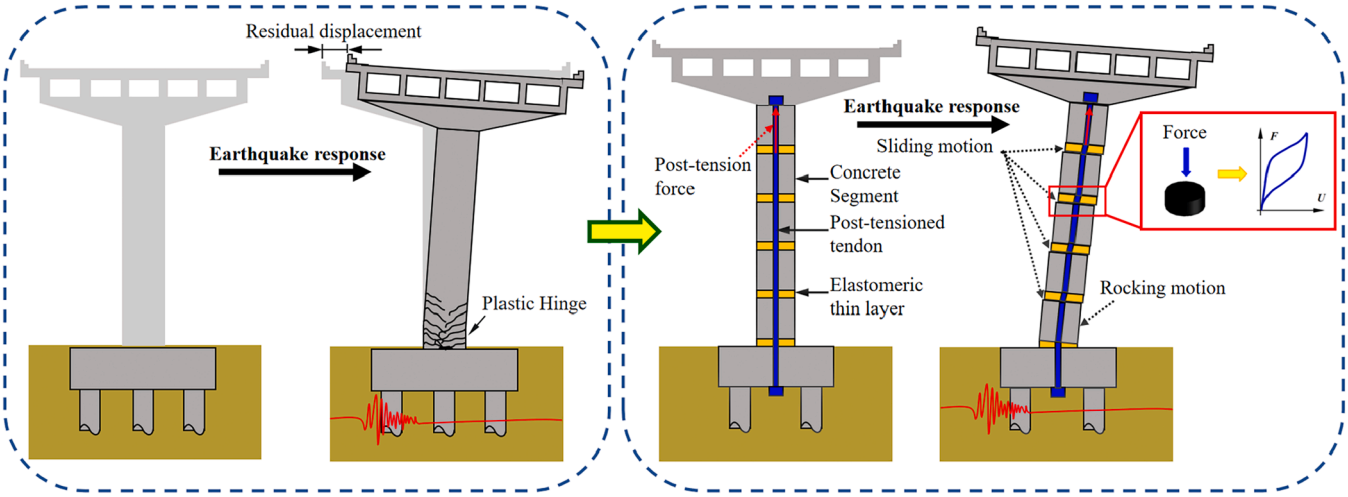

Fig. 1. Conceptual illustration of a biomechanically inspired damage-free pier system.

Table 1
Mechanical properties of the test specimens.

Category	Material	Hardness Shore A (°)	Density (g/cm³)	Elongation at Yield (%)	Elongation at Break (%)	Compression Set (%)
Amorphous polymers	TPU	80	1.22	/	610	26
	Neoprene	70	1.40	/	300	25
	Neoprene / NBR	70	1.47	/	250	20
Semi-crystalline polymers	UHMWPE	67	0.93	20	50	/
	PP	70	0.95	8	/	/
	HDPE	64	0.96	9	300	/

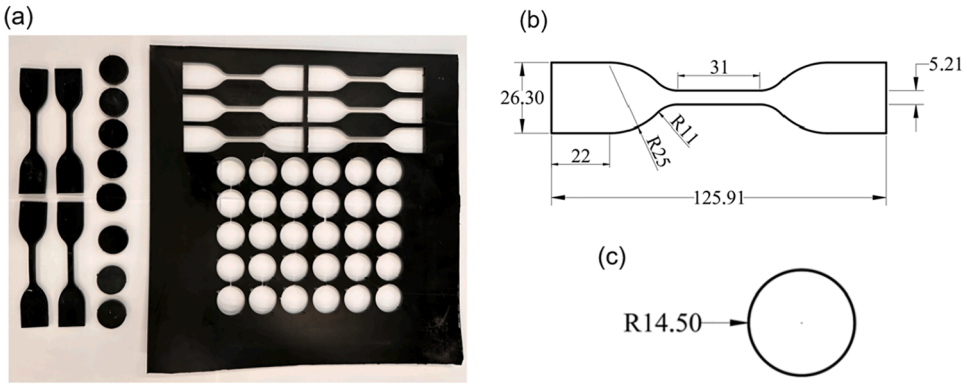

Fig. 2. (a) Overview of waterjet-cut final specimens, (b) ISO 37 Type 1 A tensile specimen geometry, and (c) ISO 7743 Type 4 compression specimen geometry (in mm).

specimens prepared in accordance with BS ISO 37:2024 [47], and the cylindrical compression specimens prepared in accordance with BS ISO 7743:2017 [48]. The ambient temperature was held at 15 °C for all tests. To meet the standard-specified specimen height of 12 mm for cylindrical compression tests, four circular discs (each 3 mm thick) were stacked and aligned carefully to form a single specimen, the discs were compressed between flat steel loading shims, where the normal compressive force generated sufficient interfacial friction between layers to prevent slip during testing.

2.2. Experimental setup

All tests were conducted at the Testing and Structures Research Laboratory (TSRL) at the University of Southampton. Fig. 3 presents the experimental setup and equipment. Tensile tests were performed using an Instron Electropuls E10000 testing machine (10 kN capacity), with custom loading histories programmed through the WaveMatrix2 software and executed via the PC-based Instron Console control system. Considering that large displacements during testing can lead to the failure of conventional strain gauges or extensometers, a non-contact optical method based on video extensometer was employed to measure the tensile strain. Two tracking markers were applied within the gauge section of the specimen to enable accurate point tracking over a central 25 mm deformation region. In addition, horizontal lines were drawn 38 mm from each end of the specimen to assist with fixture alignment. The deformation process was recorded by an imaging system comprising a Manta G504-B industrial camera (Allied Vision, Stadtroda, Germany) and a Nikon AF 50 mm f/1.8D lens (Japan), with the frame rate set at 5 Hz. The captured image data were transferred via Ethernet to a computer equipped with the MatchID Stereo software (MatchID, Ghent, Belgium) for image processing and analysis, from which the strain within the gauge length was calculated. This technique has been demonstrated to be a reliable method [49,50].

Compression tests were performed using an Instron 8802 (capacity 250 kN). During testing, the specimens were placed between two thin steel plate shims. To reduce the influence of friction on the test results, a

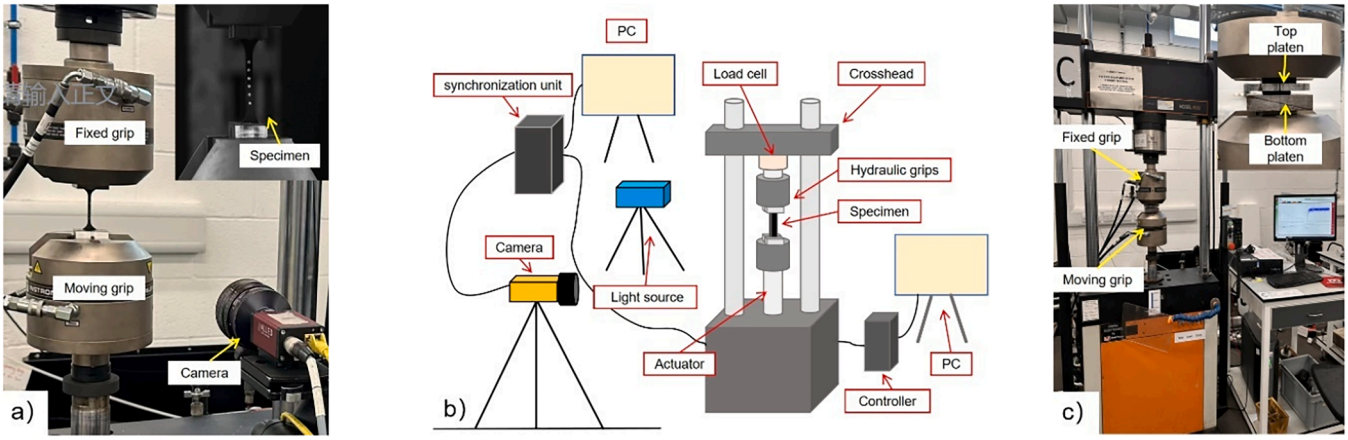

Fig. 3. (a) Tensile test gripping system and detailed view of the marked points on the tensile specimen; (b) Digital Image Correlation (DIC) setup used for point tracking; (c) Compression test fixture and detailed view of the compression specimen.

layer of lubricant grease was applied to the contact surfaces between the specimen ends and the steel plates.

2.3. Loading protocol

The testing programme covered the following six loading protocols: (A) Five loading–unloading cycles were applied at each strain level, followed by an incremental increase in the target strain and continued cyclic loading, to capture the stress softening behaviour of the elastomeric materials under complex strain paths; (B) Fifteen loading–unloading cycles were performed at a fixed strain level, with a 5 s hold at the peak strain in each cycle, to evaluate stress relaxation behaviour, i.e., the time-dependent viscoelastic response; (C) Similar to Protocol A but with higher strain amplitudes, this protocol aimed to investigate the stress–strain behaviour, energy dissipation, and failure modes of the materials under large deformations; (D) Five repeated loading–unloading cycles were conducted at a fixed strain level, followed by a 30 min rest period under zero stress, to assess residual strain and recovery ratio; (E) A stepwise-increasing triangular waveform loading was applied, where each cycle started at zero, increased to a predefined peak strain, and was then fully unloaded back to zero, to examine the hysteresis behaviour and instantaneous stiffness evolution of the materials under repeated and accumulated loading; (F) A stress-controlled test was conducted to monitor 24 h strain creep, enabling evaluation and prediction of the long-term time-dependent behaviour of the materials.

The loading protocols developed in this study are designed to capture the fundamental nonlinear tensile and compressive behaviour of the candidate materials. Although these materials are ultimately intended for application in compressive components, tensile testing remains essential. This is because a complete loading–unloading response provides a more comprehensive characterisation of the material's mechanical performance, offering valuable insight into failure modes, underlying microphysical deformation mechanisms, and supporting the calibration of subsequent constitutive models. It should be noted that the uniaxial tension and compression tests presented in this study do not fully reproduce the stress state that nearly incompressible elastomeric materials, such as Neoprene and Neoprene/NBR, would experience when applied as thin interlayers in the proposed damage-free pier system. In practical applications, the confinement imposed by the restraint of lateral deformation due to interfacial friction would lead to a multiaxial stress state characterised by high hydrostatic pressures and elevated shear stresses near the elastomer–concrete interfaces, similar to the behaviour observed in multilayer elastomeric bearings. For the TPU and semi-crystalline polymer materials considered in this study, the uniaxial loading conditions are more representative of the stress states expected in the intended application, and the presented tests provide a reasonable approximation of their in-service mechanical behaviour. The objective of the present experimental programme is therefore not to directly replicate the fully confined boundary conditions relevant to Neoprene-based materials, but to provide a fundamental characterisation and comparison of the intrinsic material behaviour under controlled loading paths of the selected materials.

The large strain amplitudes applied in the experiments (up to 80 %) allow for the assessment of material behaviour under extreme local deformation, simulating the high strain demands expected during strong seismic events. This aspect represents a key strength of the present study and addresses the gap identified earlier. Detailed analyses of the unique responses observed under rapid and large amplitude loading conditions are presented in Sections 3.3 and 4.3. The strain histories used for both tensile and compressive tests are illustrated in Fig. 4. It is worth noting that, in an actual segmental self-centring rocking column, the elastomeric layers will predominantly experience compression.

3. Experimental results and discussion of tensile tests

3.1. Stress softening tests

Fig. 5 presents the nominal stress–strain hysteresis curves of the six materials under loading protocol A with a strain rate of 0.01/s, as commonly used in previous studies [37,39]. All materials exhibited significantly greater stress softening during the first cycle at each strain level compared to subsequent cycles. Fig. 5(a) shows that that Neoprene rubber and Neoprene/NBR rubber displayed similar elastic modulus and yield-like stress, and their loading–unloading curves showed near-elastic behaviour throughout. Under tensile loading, the rubber molecular chains gradually transform from an initially disordered configuration to a more aligned arrangement [35,51]. TPU exhibited higher elastic modulus and yield-like stress than the aforementioned rubbers. In TPU, the soft segments impart rubber-like behaviour, while the hard segments function as physical crosslinks, playing a role akin to the chemical crosslinks found in vulcanised rubber, thus governing the hysteresis, permanent deformation, and tensile strength of the material [37].

The semi-crystalline polymer materials (UHMWPE, PP and HDPE) demonstrated a characteristically nonlinear stress–strain response (Fig. 5(b)). The initial stage exhibits a nearly elastic response, followed by a gradual transition into yielding [39]. It is widely accepted that the deformation behaviour of crystalline polymers is governed more by intermolecular forces than by covalent C–C bonds [33]. As shown in Fig. 5(b), both PP and UHMWPE demonstrated robust stress retention during the plastic flow stage, suggesting that increased molecular weight in polyethylene and the presence of methyl side groups in polypropylene help resist crystalline break-up or excessive amorphous phase stretching. It is worth noting that increasing the molecular weight of polypropylene may hinder crystallisation and deteriorate mechanical performance [52]. Moreover, it was observed that, among the polyethylene materials (UHMWPE and HDPE), the stress softening effect diminished progressively with increasing strain level, whereas the PP appeared unaffected by this phenomenon.

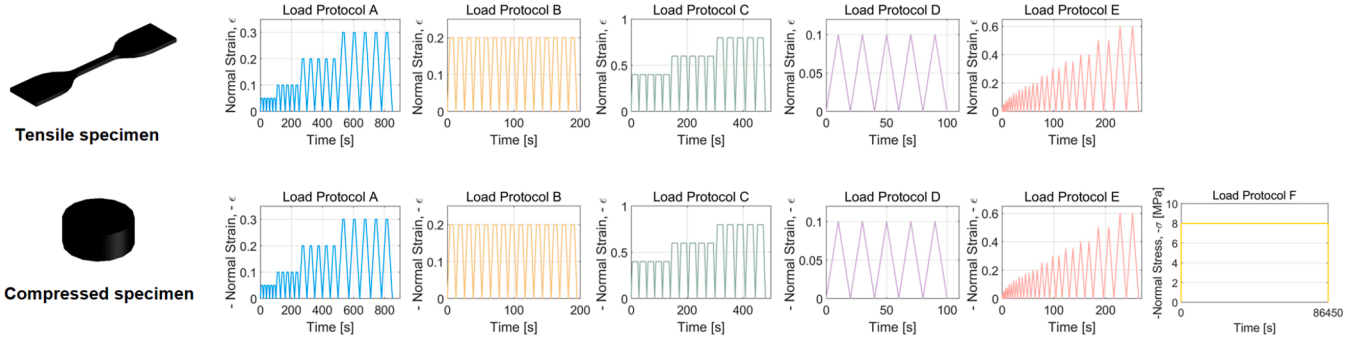

Fig. 4. Loading histories for the tensile and compression tests.

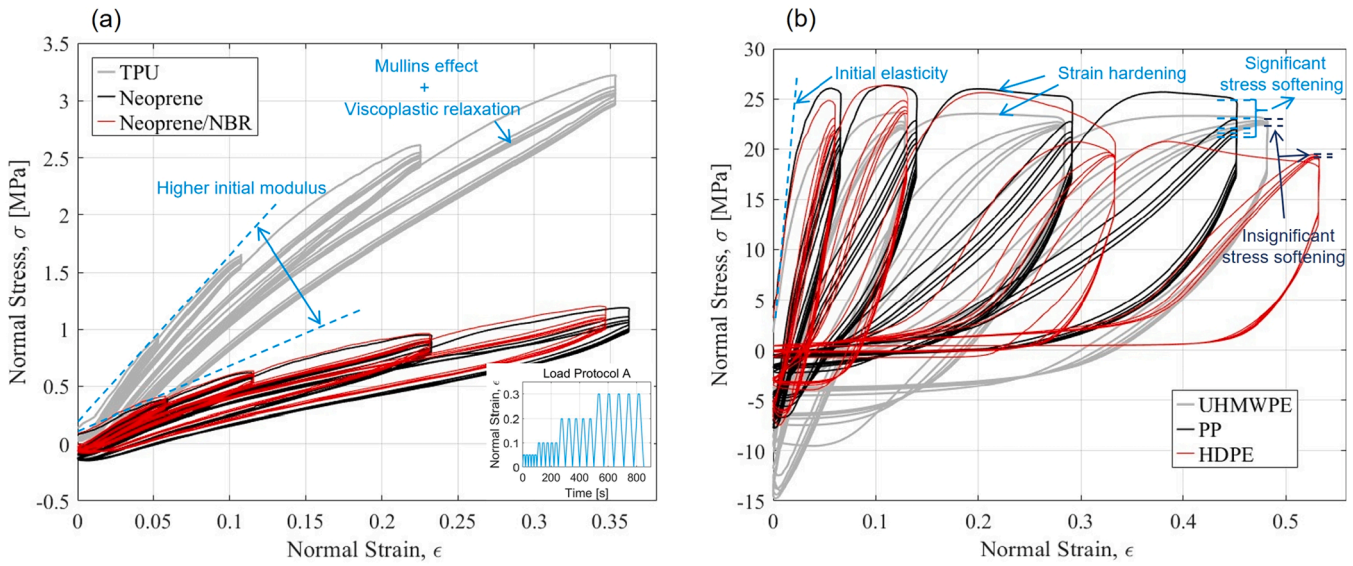

Fig. 5. Stress–strain hysteresis curves under tensile loading protocol A: (a) TPU, Neoprene and Neoprene/NBR; (b) UHMWPE, PP and HDPE.

3.2. Transient relaxation tests

Fig. 6 presents the nominal stress–strain hysteresis curves of the tested specimens under loading protocol B with a strain rate of 0.05/s, as commonly used in previous studies [37]. During each holding period, all elastomeric materials exhibited a decrease in stress over time. As time progressed, the rate of stress relaxation gradually slowed down until the stress eventually stabilised. It is worth noting that although semi-crystalline polymer materials showed higher initial stresses, they also experienced more significant relaxation compared to the amorphous polymers (Fig. 6(a) vs Fig. 6(b)). This relaxation behaviour is sometimes referred to as microstructural relaxation [53]. According to conventional elasto-plastic theory, if no new deformation occurs during cyclic loading, the subsequent cycles—prior to the onset of new plastic deformation—are governed by viscoelastic mechanisms. Recent studies by Reyes et al. [44] have demonstrated that this principle also applies to amorphous polymers.

3.3. Hysteresis curve under large strain tests

Fig. 7 shows the nominal stress–strain hysteresis curves of the six materials under loading protocol C with a strain rate of 0.1/s. Fig. 7(a) shows that amorphous polymers exhibit more pronounced nonlinearity and slight strain hardening during loading. This is attributed to the gradual straightening of disordered rubber molecular chains [51]. In the case of TPU, the hard segments undergo chain disentanglement while the soft segments align and stretch progressively [37]. Additionally, it was observed that the elongation strain at the central gauge marks of rubber specimens was smaller than that of TPU, opposite to the trend seen under low strain rate loading. One possible explanation is that rubber is more rate-sensitive. At higher tensile speeds, the internal molecular chains do not have sufficient time to stretch and reorient. As a result, greater external force is required to achieve the same elongation compared to slower tensile rates [54].

For semi-crystalline polymers, HDPE and PP fractured at strain levels of approximately 75 % and 125 %, respectively (Fig. 7(b)). Fig. 8 presents images of HDPE and PP 0.2 s before and immediately after

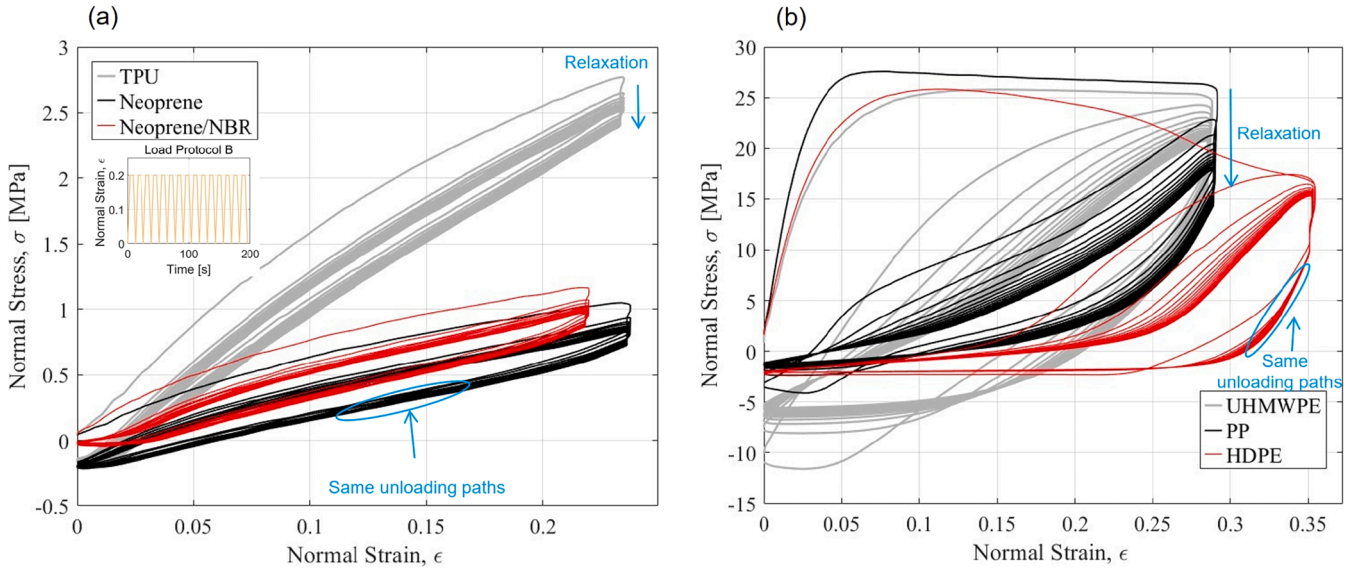

Fig. 6. Stress–strain hysteresis curves under tensile loading protocol B: (a) TPU, Neoprene and Neoprene/NBR; (b) UHMWPE, PP and HDPE.

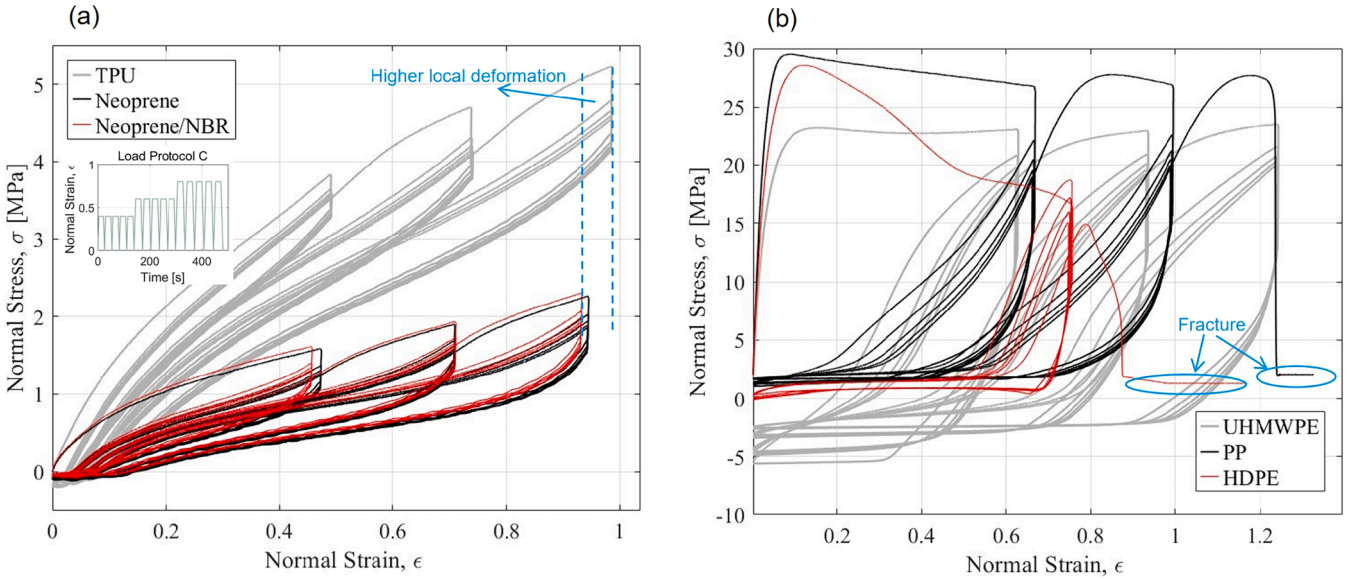

Fig. 7. Stress–strain hysteresis curves under tensile loading protocol C: (a) TPU, Neoprene and Neoprene/NBR; (b) UHMWPE, PP and HDPE.

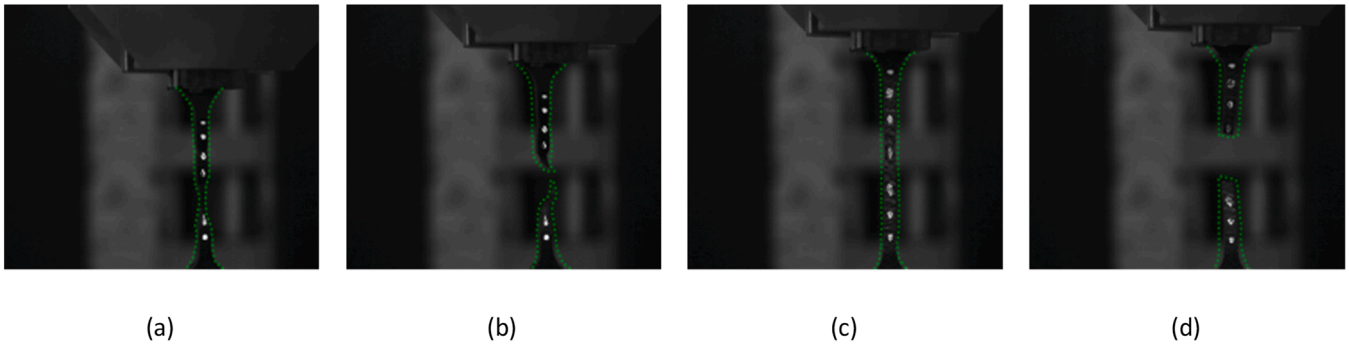

Fig. 8. (a) HDPE specimen 0.2 s before fracture; (b) HDPE specimen after failure; (c) PP specimen 0.2 s before fracture; (d) PP specimen after failure.

fracture. The failure modes of the two materials are clearly distinct: HDPE displayed noticeable necking prior to fracture, while PP showed visible fatigue crack propagation zones on the fracture surface. The former corresponds to a necking-induced failure under high strain, whereas the latter is indicative of fatigue failure, consistent with the findings reported by Qi et al. [40]. It is worth noting that in both cases,

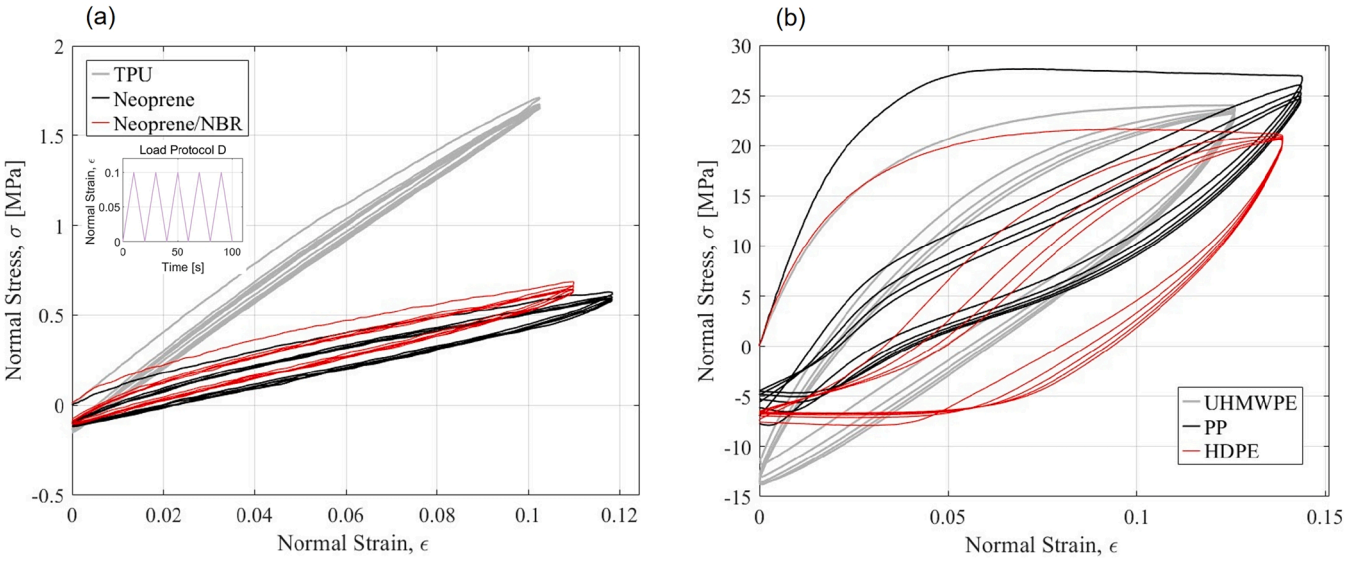

Fig. 9. Stress–strain hysteresis curves under tensile loading protocol D: (a) TPU, Neoprene and Neoprene/NBR; (b) UHMWPE, PP and HDPE.

fracture occurred during the strain-holding phase.

3.4. Strain recovery tests

Fig. 9 shows the nominal stress–strain hysteresis curves of the specimens under loading protocol D with a strain rate of 0.01/s. Table 2 summarises the residual strain and strain recovery of the specimens. As shown in Table 2, TPU exhibited the smallest residual strain and the highest recovery ratio, achieving 73.3 % residual strain recovery within 30 min and leaving a residual strain of only 0.004, demonstrating excellent elastic recovery performance. Among the rubber materials, Neoprene/NBR rubber showed a smaller residual strain and higher recovery ratio than Neoprene rubber. In contrast, the semi-crystalline polymers (UHMWPE, PP and HDPE) exhibited significantly lower strain recovery (38 %, 15 %, and 7 %, respectively) within the same recovery period. It is worth noting that semi-crystalline polymers undergo plastic deformation during tension, leading to an irreversible increase in length. Due to their higher stiffness, noticeable compressive stress appears on the stress–strain curve during unloading. In contrast, amorphous polymers are more elastic, with smaller residual deformation, and thus produce almost no compressive stress during unloading.

3.5. Cyclic loading with increasing amplitude tests

Fig. 10 presents the nominal stress–strain hysteresis curves of the materials under loading protocol E with a strain rate of 0.05/s. At each strain level, the area enclosed by the hysteresis loop in the first loading cycle was consistently larger than that of the subsequent cycles. As the peak strain increased progressively, all materials exhibited larger hysteresis loops (greater energy dissipation), except for HDPE, which fractured at 70 % strain. A detailed quantitative analysis and comparison of energy dissipation will be presented in Section 4.3. Upon examining the hysteresis loops of all tested materials, it was consistently observed that the peak stress reached during the first loading cycle at each strain level closely approaches the peak stress attained during the first loading of the previous strain level [38]. This indicates that as the strain level increases, the specimens require greater deformation to reach a similar stress level as observed in the preceding cycle. Additionally, for all materials, the loading path during each cycle closely approached the unloading path from the previous cycle (as shown in Fig. 10(b)), and the unloading paths remained highly consistent across cycles. This indicates that the primary residual strain accumulation occurred during the first loading cycle at each level, while subsequent cycles did not produce significant additional residual deformation.

4. Experimental results and discussion of compressive tests

4.1. Multi-step relaxation and stress softening tests

Fig. 11 shows the nominal stress–strain hysteresis curves of the specimens under loading protocol A with a strain rate of 0.01/s. The stress–strain responses are compressive in nature but are plotted in the positive direction for simplicity and consistency. Table 3 summarises the maximum peak stresses ($\sigma_{1,Max}$ and $\sigma_{5,Max}$) in the first and fifth loading cycles of the 5 %, 10 %, 20 %, and 30 % strain level respectively, and their stress retention ratio ($\sigma_{5,Max}$ / $\sigma_{1,Max}$). As observed in the tensile tests, TPU continued to exhibit a higher initial modulus and yield stress compared to the other rubber materials. Furthermore, the degree of stress softening in TPU was significantly lower than that observed in both the rubber materials and the semi-crystalline polymers. When the applied strain increased from 5 % to 30 % (see Table 3), TPU demonstrated the highest stress retention ratio, ranging from 94.7 % to 97.7 %, indicating a near-elastic and stable response. In contrast, Neoprene/NBR rubber showed a more pronounced softening trend, with the lowest stress retention ratio (77.4 %–88.9 %). This softening behaviour is primarily governed by the Mullins effect, in which the initial loading beyond the material's previous maximum strain leads to microstructural damage caused by polymer chain slippage or filler–polymer interface debonding [53], resulting in a significant reduction in stress during subsequent loading. A similar softening phenomenon was observed in Neoprene rubber, which exhibited more notable stress softening compared to TPU.

For the semi-crystalline polymers, UHMWPE exhibited a high stress retention ratio of 94.3 %–95.7 % at a maximum strain of 30 % and 20 %, respectively, which can be primarily attributed to its extremely long molecular chains that confer exceptional toughness and strong adaptive strain capacity. In comparison, HDPE showed slightly lower performance, confirming that longer molecular chains have a positive effect on resisting stress softening. For PP, however, exhibited a lower stress retention ratio (82.4 %–88.2 %). This is attributed to the superior chain flexibility and structural regularity of polyethylene (PE), which allows the molecular chains to fold and stack repeatedly to form crystalline regions more readily. In contrast, each backbone carbon atom in PP carries a side methyl group (–CH_3), preventing the formation of a tightly packed crystalline structure as seen in polyethylene [55]. As a result, PP exhibits lower crystallinity and density than PE and is more prone to microcracking and local chain slippage under repeated cyclic loading.

Fig. 12 illustrates the trend of stress retention ratio of each material as a function of increasing strain levels. Within the lower strain range (5 %–10 %), differences among the materials were relatively minor. However, as the strain increased to 20 %–30 %, a polarised divergence in softening behaviour was observed between materials of different types. Amorphous polymers showed a notable decrease in normalised peak stress. For example, the Neoprene/NBR exhibited a drop of approximately 14 % in stress retention ratio when the strain increased from 10 % to 20 %, primarily due to the progressive stress degradation associated with the Mullins effect. Semi-crystalline polymers exhibited an increasing trend in stress retention ratio with increasing strain levels (Fig. 12). For instance, in the case of HDPE, the ratio increased by approximately 9 % from 10 % to 20 % strain, reaching from 84.8 % to 93.4 %.

4.2. Long-term cyclic transient relaxation tests

Fig. 13 presents the full-cycle stress–strain hysteresis curves of the six elastomeric material specimens under loading protocol B with a strain rate of 0.05/s. Fig. 14 plots the relative stress relaxation ratio R_i of each material as a function of the number of loading cycles, where $R_i = (\sigma_{i,max} - \sigma_{i,min}) / \sigma_{i,max}$ represents the relative stress relaxation at the i^{th} loading cycle, and $\sigma_{i,max}$ and $\sigma_{i,min}$ are the peak and minimum stresses, respectively, during the holding period at the target strain level. During repeated cycling at a constant strain level, a gradual stabilisation of the stress relaxation response was observed. From the long-term cyclic behaviour, TPU exhibited the lowest overall relaxation response. It reached a steady state immediately after the first cycle, with the relative

Table 2
Summary of strain-recovery response.

Material	TPU	Neoprene	Neoprene/NBR	UHMWPE	PP	HDPE
Residual Strain	0.015	0.037	0.019	0.029	0.026	0.056
Residual Strain after 30 mins	0.004	0.019	0.007	0.018	0.022	0.052
Total Recovery (%)	73.333	48.649	63.158	37.931	15.385	7.143

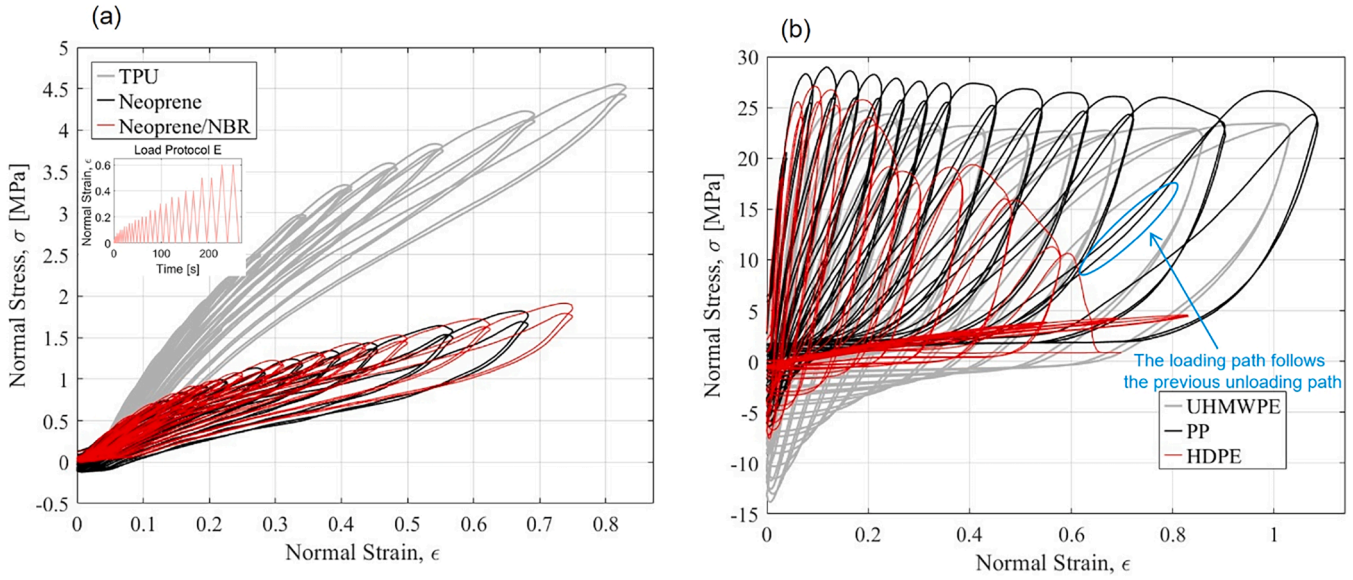

Fig. 10. Stress–strain hysteresis curves under tensile loading protocol E: (a) TPU, Neoprene and Neoprene/NBR; (b) UHMWPE, PP and HDPE.

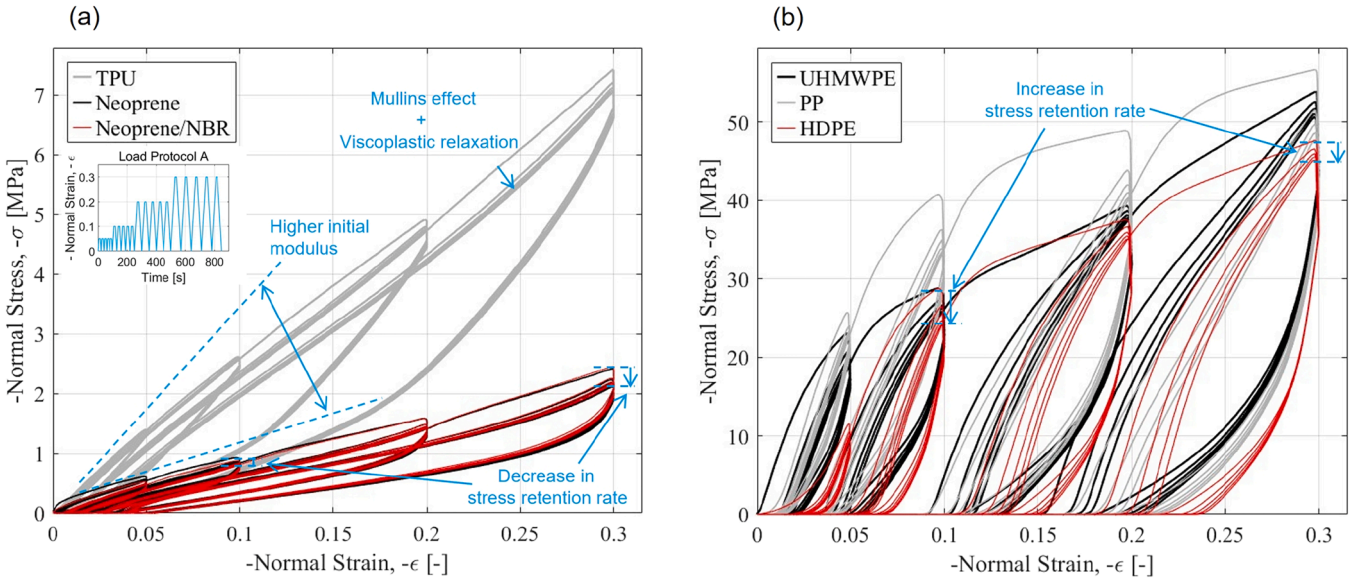

Fig. 11. Stress–strain hysteresis curves under compressive loading protocol A: (a) TPU, Neoprene and Neoprene/NBR; (b) UHMWPE, PP and HDPE.

Table 3
Maximum peak stresses in the first and fifth loading cycles of the 5 %, 10 %, 20 %, and 30 % strain level respectively, and stress retention ratio ($\sigma_{1,Max}$, $\sigma_{5,Max}$ and $\sigma_{5,Max}$ / $\sigma_{1,Max}$) for the six materials.

Strain (%)	Material	TPU	Neoprene	Neoprene/NBR	UHMWPE	PP	HDPE
5	$\sigma_{1,Max}$ (MPa)	1.4	0.83	0.81	23.2	25.91	11.65
	$\sigma_{5,Max}$ (MPa)	1.37	0.69	0.72	19.01	22.84	9.73
	$\sigma_{5,Max}$ / $\sigma_{1,Max}$ (%)	97.7	83.1	88.9	81.9	88.2	83.5
10	$\sigma_{1,Max}$ (MPa)	2.62	1.44	1.66	28.96	40.99	28.97
	$\sigma_{5,Max}$ (MPa)	2.58	1.17	1.45	25.95	33.78	24.56
	$\sigma_{5,Max}$ / $\sigma_{1,Max}$ (%)	98.7	81.3	87.3	89.6	82.4	84.8
20	$\sigma_{1,Max}$ (MPa)	4.92	2.75	3.8	39.47	49.02	37.67
	$\sigma_{5,Max}$ (MPa)	4.73	2.19	2.78	37.77	40.67	35.17
	$\sigma_{5,Max}$ / $\sigma_{1,Max}$ (%)	96.2	79.6	73.2	95.7	83.0	93.4
30	$\sigma_{1,Max}$ (MPa)	7.44	5.13	7.44	53.98	56.72	47.62
	$\sigma_{5,Max}$ (MPa)	7.05	4.02	5.76	50.9	47.86	45.23
	$\sigma_{5,Max}$ / $\sigma_{1,Max}$ (%)	94.7	78.4	77.4	94.3	84.4	95.0

relaxation ratio maintained within a narrow range of 7.2–7.7 %. Neoprene rubber and Neoprene/NBR rubber showed similar relaxation

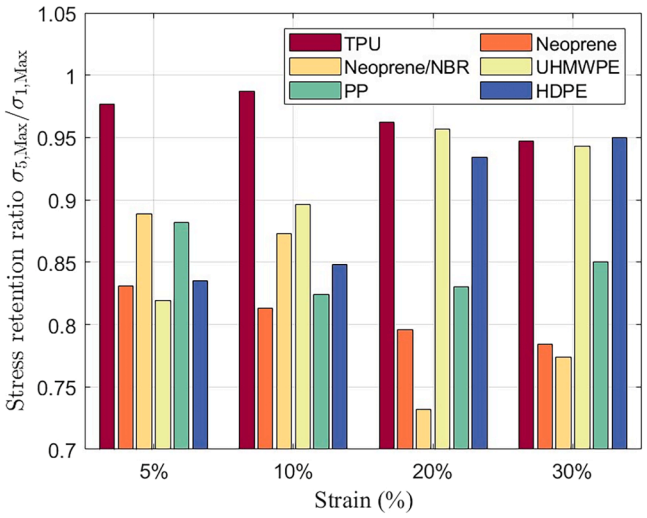

Fig. 12. Bar chart showing the peak compressive stress retention ratio ($\sigma_{5,Max}$ / $\sigma_{1,Max}$) as a function of increasing maximum nominal strain for the different materials.

behaviour, stabilising quickly after the second cycle, with relative relaxation ratios fluctuating around 16 % and 17 %, respectively. In contrast, semi-crystalline polymers, UHMWPE, PP, and HDPE, required more cycles to approach a stable relaxation response. Even by the 15th cycle, a slight downward trend was still observable, which is consistent with the cumulative damage effects associated with the pronounced stress softening mechanisms previously observed. This was particularly evident in PP, where the relative relaxation ratio remained as high as 22 % at the end of the final cycle. In summary, under seismic conditions, materials with low relaxation response can maintain more stable load bearing and energy dissipation capacities throughout the earthquake, thereby reducing cumulative residual displacements caused by strength degradation. Therefore, TPU offers significant advantages in enhancing the post-earthquake recoverability of segmental piers.

4.3. Analysis of energy dissipation and residual deformation under large strains tests

Fig. 15 shows the nominal stress–strain hysteresis curves from the compression tests conducted under loading protocol C with a strain rate of 0.1/s. It is evident that the change in strain level led to nonlinear behaviour in the amorphous polymers. As the strain increased, the initial modulus and yield-like stress of TPU became progressively lower than those of Neoprene/NBR rubber. The unloading path exhibited a large, highly nonlinear hysteresis loop, with most of the strain recovered during unloading. For semi-crystalline polymers, a distinct stress–strain response was observed at small strains: an initial elastic response followed by a relatively stable strain-hardening phase after reaching the yield point. As strain increased, the yield turning point became less distinguishable, and the degree of strain hardening intensified. After unloading, semi-crystalline polymers showed significant residual deformation, with residual strains generally exceeding 0.6. As shown in Fig. 16, the semi-crystalline polymers exhibited considerable permanent plastic deformation, while the amorphous polymers experienced smaller residual strains and recovered more rapidly.

Fig. 17(a–f) shows the evolution of energy dissipation during cyclic loading for each material as a function of increasing strain under the loading protocol C. The dissipated energy was calculated by integrating the area enclosed by the hysteresis loops at each cycle and then

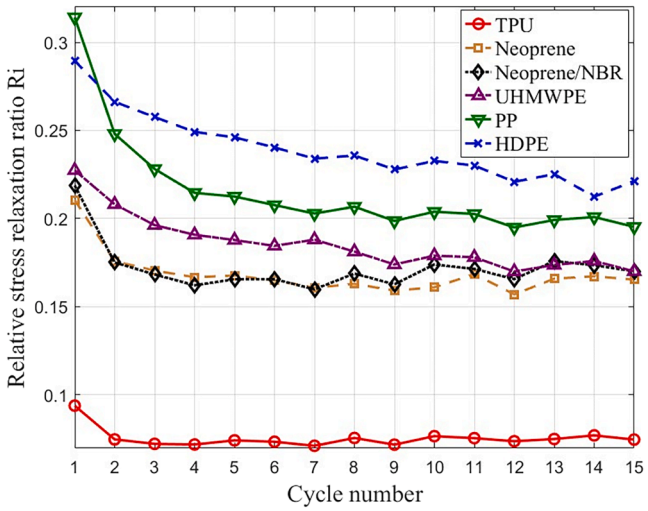

Fig. 14. Evolution of the relative compressive stress relaxation ratio as a function of loading cycle number for the different materials.

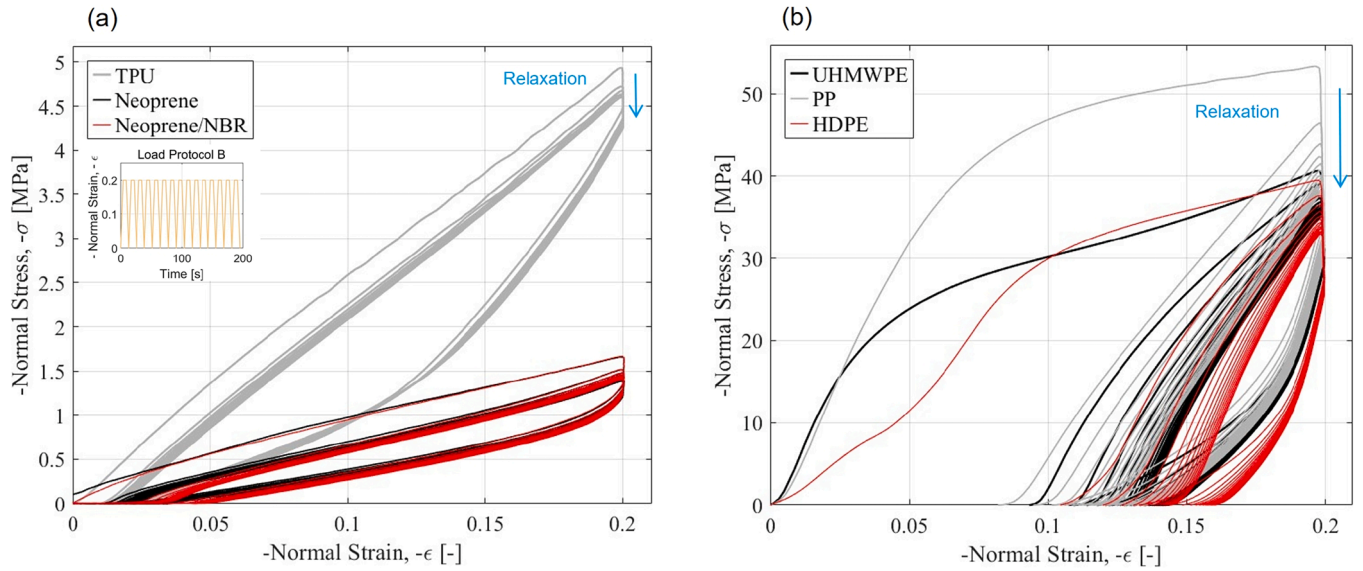

Fig. 13. Stress–strain hysteresis curves under compressive loading protocol B: (a) TPU, Neoprene and Neoprene/NBR; (b) UHMWPE, PP and HDPE.

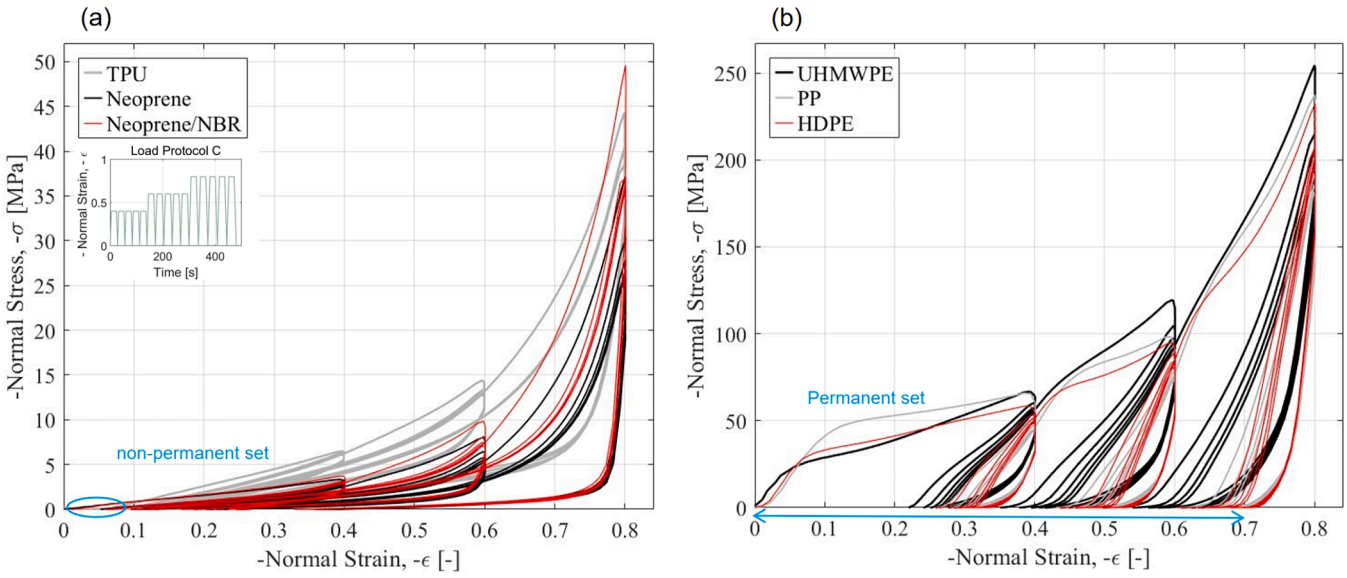

Fig. 15. Stress–strain hysteresis curves under compressive loading protocol C: (a) TPU, Neoprene and Neoprene/NBR; (b) UHMWPE, PP and HDPE.

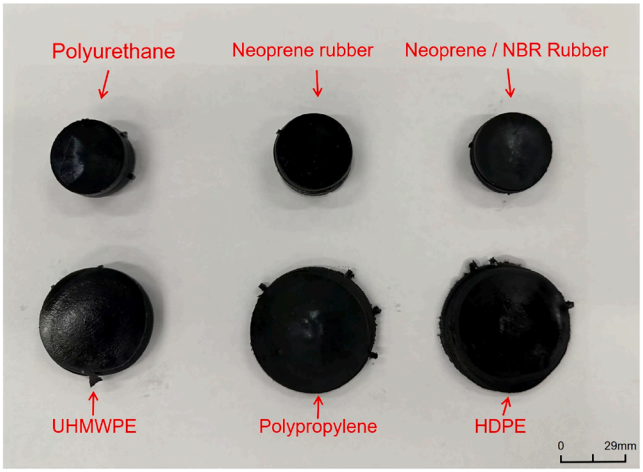

Fig. 16. Residual deformation of the six materials after compressive unloading.

normalised to the total dissipated energy of each corresponding material. All materials exhibited the highest energy dissipation in the first cycle, followed by a gradual stabilisation in subsequent cycles. Notably, the amorphous polymers maintained relatively large and stable energy dissipation across repeated cycles at each strain level, whereas the semi-crystalline polymers showed a significant decline and degradation trend in dissipative capacity with continued loading. Fig. 17(g) presents the total cumulative dissipated energy of all materials, normalised by the total energy dissipated by UHMWPE.

The energy dissipation capacity of Neoprene rubber was found to be the lowest among the materials tested. In contrast, the Neoprene/NBR rubber exhibited approximately 40 % higher energy dissipation than Neoprene rubber, owing to the presence of polar side groups (–CN and –Cl), which introduce stronger intermolecular forces and internal friction [56]. TPU outperformed both rubbers in terms of energy dissipation and also exhibited the smallest residual deformation. Among the semi-crystalline polymers, UHMWPE showed significantly higher energy dissipation than HDPE. This is primarily attributed to its higher molecular weight, which leads to a greater number of entanglement and attraction points between molecular chains. These factors hinder chain mobility, increasing mechanical hysteresis and thus energy dissipation. PP also demonstrated a relatively high energy dissipation capacity. However, this enhanced dissipation comes at the cost of irreversible plastic deformation, as a substantial portion of the dissipated energy is converted into heat.

4.4. *Recovery of residual deformation tests*

Fig. 18 shows the nominal stress–strain hysteresis curves from the compression tests conducted under loading protocol D with a strain rate of 0.01/s. Table 4 provides the residual deformation recovery data for each specimen. Under small-strain loading conditions, the amorphous polymers recovered most of their deformation within 30 min, indicating that their deformation mechanisms were primarily governed by recoverable viscoelastic effects. Among them, TPU exhibited the most favourable elastic recovery performance. For the semi-crystalline polymers, PP exhibited the highest recovery rate after 30 min, followed by HDPE and UHMWPE. Notably, HDPE showed only a 7 % recovery rate under tensile loading, suggesting an unusual dependence of recovery behaviour on the mode of deformation at low strain levels, an observation that also applies to other semi-crystalline polymers. It is worth noting that, in practical applications, prestressing tendon (PT) could be introduced to provide a self-centring capability while allowing semi-crystalline polymers to maintain their high energy dissipation capacity, thereby enhancing both seismic resilience and re-centring performance of the system.

4.5. *Hysteresis curves under increasing amplitude tests*

Fig. 19 shows the nominal stress–strain hysteresis curves from the compression tests conducted under loading protocol E with a strain rate of 0.05/s. This section evaluates the variation of instantaneous stiffness modulus in specimens subjected to triangular loading with incrementally increasing strain levels. Instantaneous stiffness modulus was calculated as the secant slope near the peak points on the stress–strain curves during each loading cycle. As shown in Fig. 19, the loading path of TPU follows a gradual, exponential-like increase similar to that of rubber materials. In contrast, the semi-crystalline polymers exhibited distinctly different loading behaviour: when the applied strain exceeded the previous maximum, the curves transitioned from a linear elastic phase to a plastic dissipation phase. In the second repeated loading cycle, the stress response throughout the entire cycle closely followed the previous elastic loading path.

To more intuitively compare the evolution of instantaneous stiffness

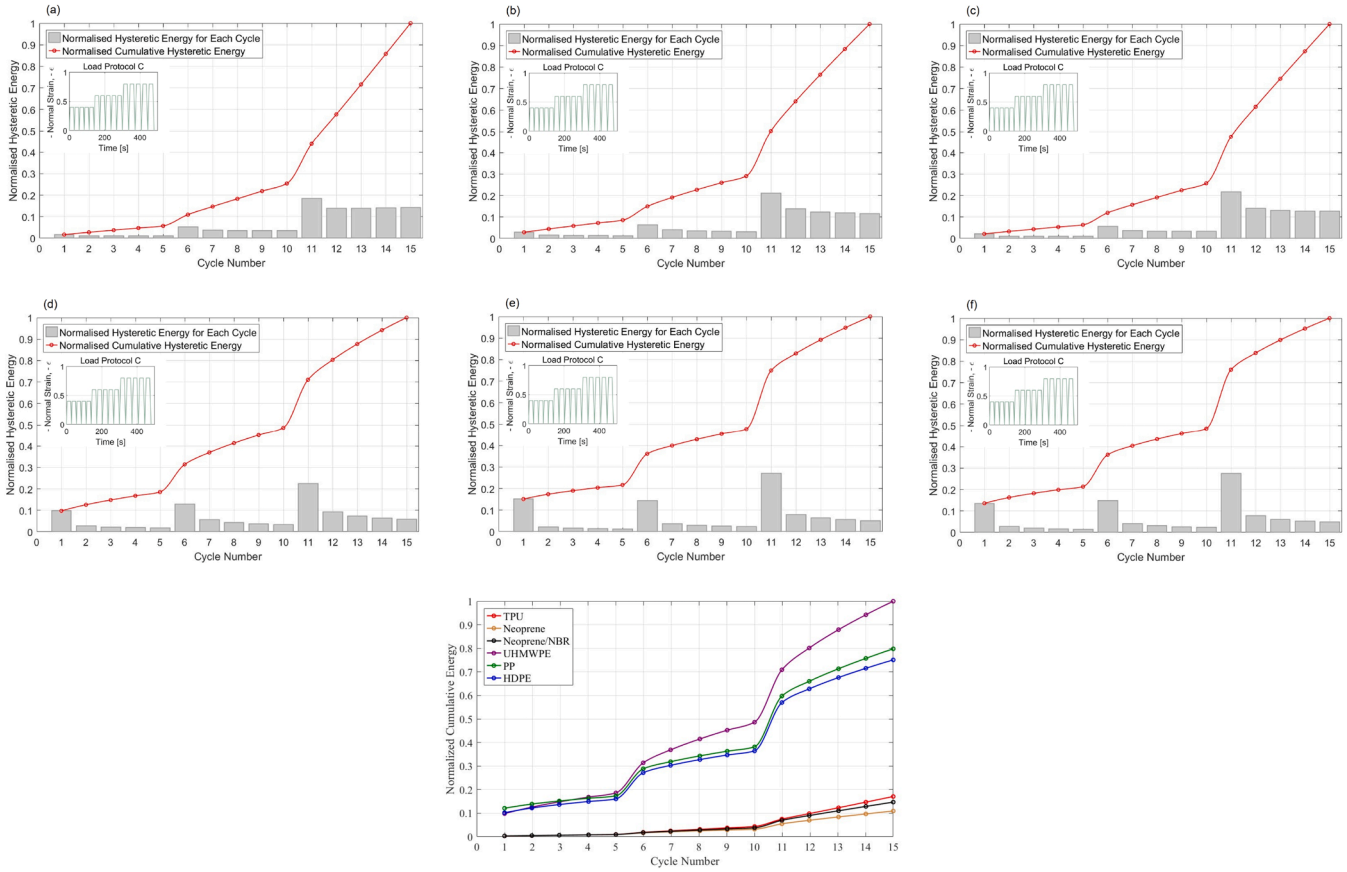

Fig. 17. Hysteretic energy dissipation under compressive loading: (a) TPU; (b) Neoprene; (c) Neoprene/NBR; (d) UHMWPE; (e) PP; (f) HDPE; and (g) all materials compared.

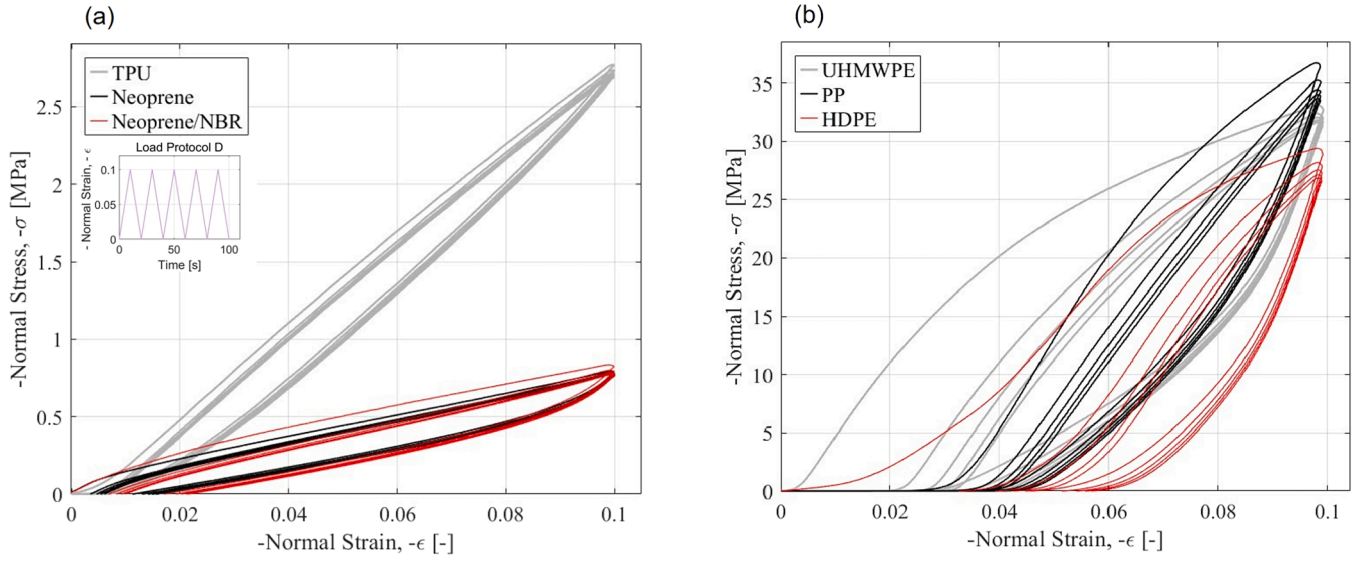

Fig. 18. Stress–strain hysteresis curves under compressive loading protocol D: (a) TPU, Neoprene and Neoprene/NBR; (b) UHMWPE, PP and HDPE.

modulus across different material types, Fig. 20 plots the instantaneous stiffness modulus versus strain during the loading phase for representative materials, TPU and UHMWPE. As shown in Fig. 20(a), TPU exhibited a rapid increase in instantaneous stiffness modulus at small strains, followed by a stable plateau and a gradual exponential rise. Notably, no significant difference was observed between the first and second loading cycles. Fig. 20(b) shows that UHMWPE consistently reached its peak instantaneous stiffness modulus early during the loading phase, followed by a rapid and symmetric decline. However, with increasing strain ($\varepsilon = 0.3$), the decline trend became less pronounced. Under larger strain levels ($\varepsilon = 0.6$), the instantaneous stiffness modulus displayed a W-shaped response with a slower rate of decay. Moreover, due to plastic deformation in UHMWPE, a noticeable shift occurred in the second loading cycle, yet the magnitude and evolution of

Table 4
Summary of strain recovery response for the six materials.

Material	TPU	Neoprene	Neoprene/NBR	UHMWPE	PP	HDPE
Residual Strain 30 mins	0.0114	0.0158	0.0182	0.0806	0.0334	0.0608
Residual Strain 3 days	0.0033	0.0111	0.0083	0.0573	0.0122	0.0347
Total Recovery after 30 min (%)	98.86	98.42	98.18	91.94	96.66	93.92
Total Recovery after 3 days (%)	99.67	98.89	99.17	94.27	98.78	96.53

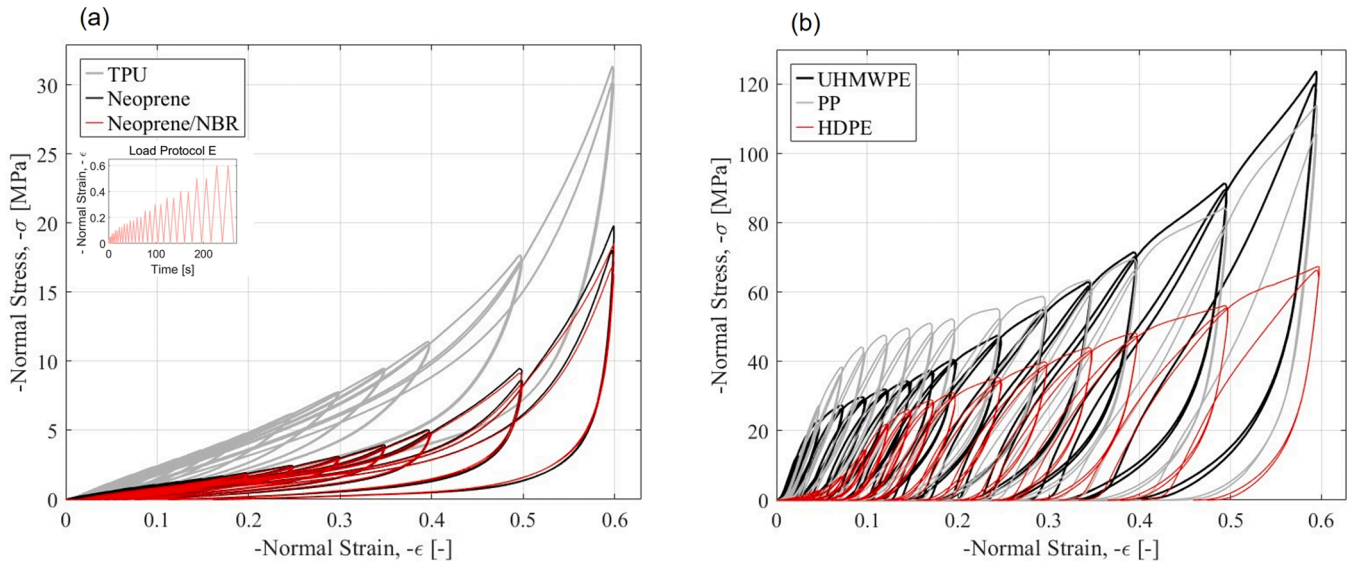

Fig. 19. Stress–strain hysteresis curves under compressive loading protocol E: (a) TPU, Neoprene and Neoprene/NBR; (b) UHMWPE, PP and HDPE.

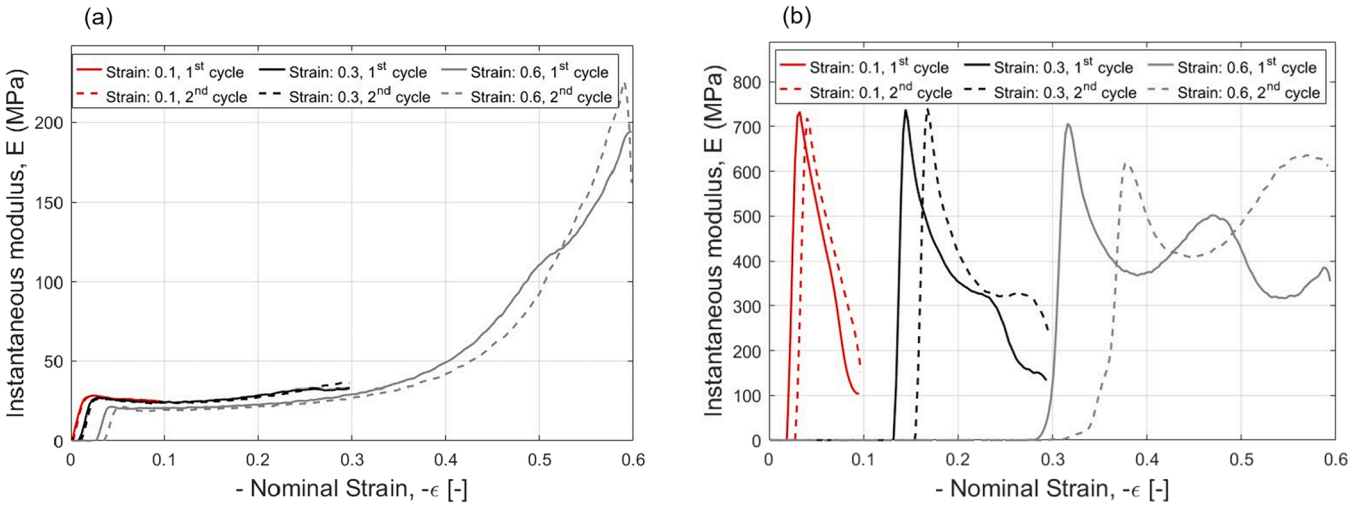

Fig. 20. Instantaneous stiffness modulus versus strain curves for selected materials: (a) TPU; (b) UHMWPE.

instantaneous stiffness modulus remained largely unaffected by the number of repeated cycles.

Fig. 21(a) presents the backbone curves formed by connecting the peak stress–strain points of each loading cycle. In conjunction with Fig. 19, it is evident that the evolution of instantaneous stiffness modulus and the residual peak strength from repeated cycles were not significantly influenced by the reduction in energy dissipation (i.e., the decrease in hysteresis loop area during the second cycle). Fig. 21(b) shows the evolution of residual strain with the number of cycles after unloading. Semi-crystalline materials generally exhibit larger residual strain, whereas amorphous polymers show comparatively smaller and a slight decreasing trend in residual strain is observed under repeated cyclic loading at the same strain amplitude.

4.6. Creep behaviour under compression

Fig. 22 shows the 24-hour creep response of the specimens under a constant compressive stress of 8 MPa in loading protocol F, plotted on a semi-logarithmic scale with strain as the measured response. It is important to note that small periodic oscillations were observed in the recorded strain response during the 24-hour creep loading process. These fluctuations are most likely attributable to the closed loop servo control of the Instron loading frame, whereby the feedback controller continuously adjusts the actuator to maintain the prescribed stress level.

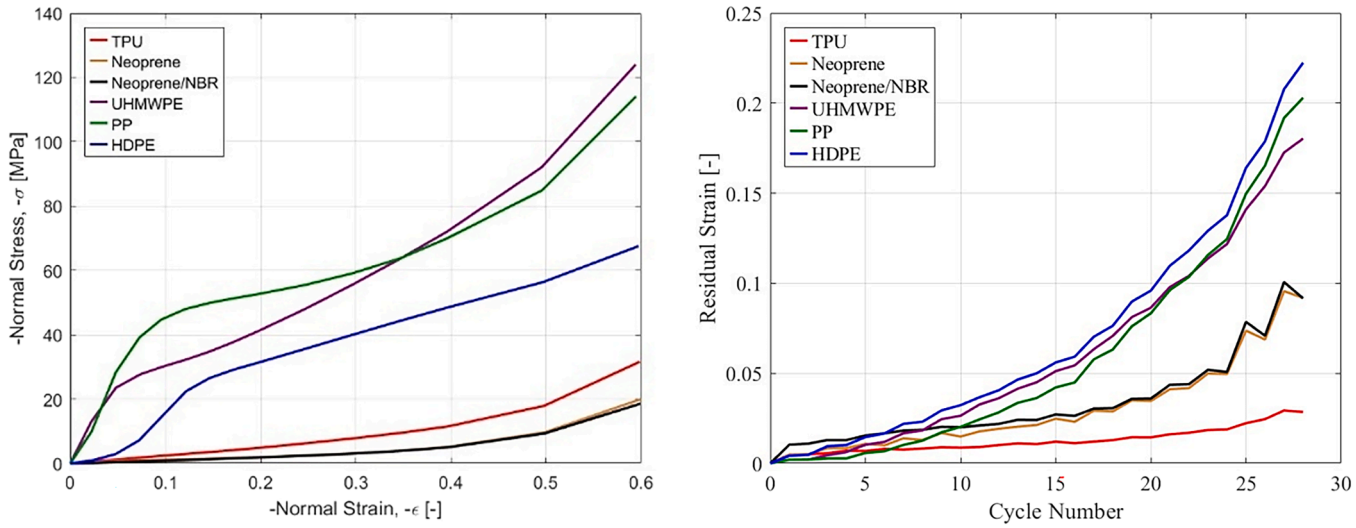

Fig. 21. Nonlinear response of all materials under compressive loading. (a) Backbone curves; (b) Residual strain.

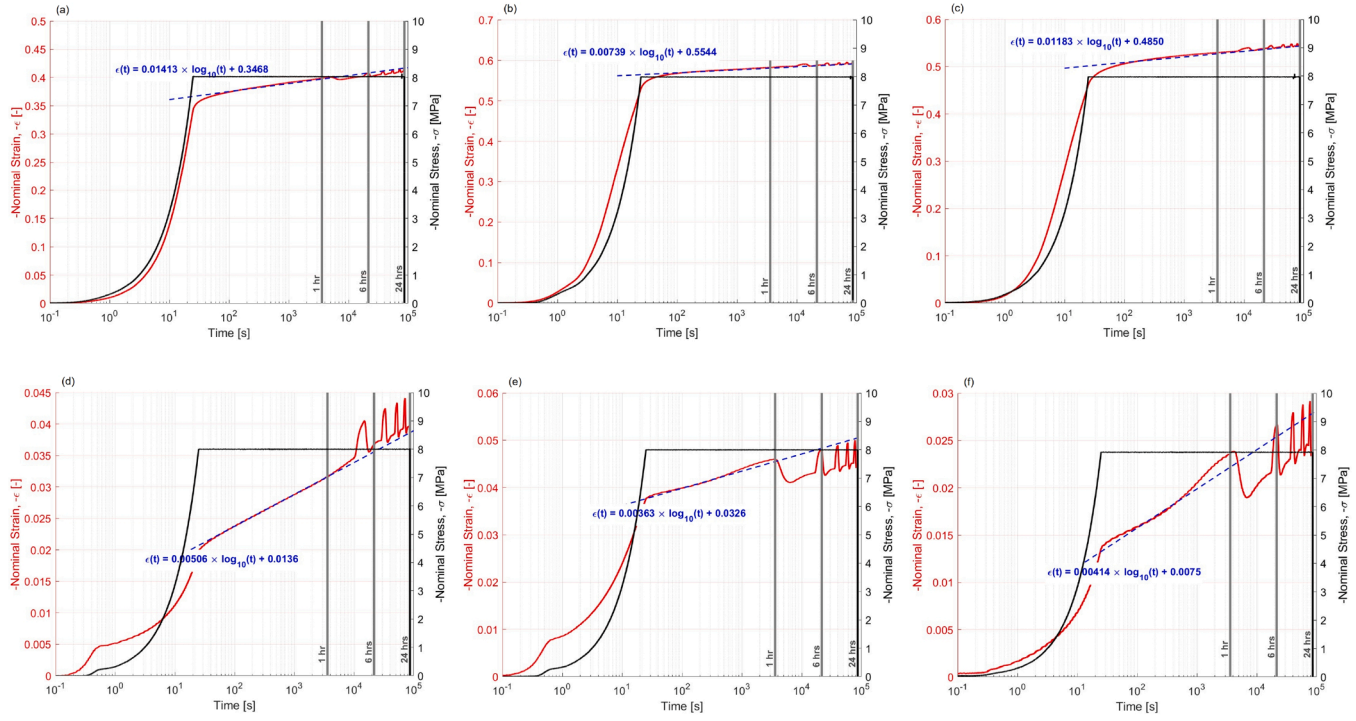

Fig. 22. Creep behaviour with reference lines at 1, 6, and 24 h: (a) TPU; (b) Neoprene; (c) Neoprene/NBR; (d) UHMWPE; (e) PP; and (f) HDPE.

This results in minor overshoots and corrections being superimposed on the underlying creep trend. The magnitude of these oscillations is negligible compared with the overall strain. A smoothed dataset (obtained by excluding these small oscillatory deviations) was therefore used to ensure that the fitted curve represents the underlying linear creep behaviour. The target stress of 8 MPa was reached at approximately 25 s. On a semi-logarithmic scale, for the amorphous polymers, the creep response beyond 50 s displayed an approximately linear trend on the semi-logarithmic scale, suggesting a stable viscoelastic mechanism. In contrast, the semi-crystalline polymers reached this linear behaviour at earlier time points, indicating that their distinct microstructures and molecular compositions govern differing creep mechanisms in this early phase. These predicted increases in strain due to long-term creep are in line with values reported in studies on polyurethane [57], rubber [58], polyethylene [59] and polypropylene [60]. In those investigations, the creep response was also observed to become roughly linear on a semi-logarithmic scale after about 10^1–10^2 seconds and this linear trend has been shown to persist for years or even decades. The present predictions provide an effective basis for comparing the long-term creep characteristics of amorphous and semi-crystalline polymers. Nevertheless, additional long-term or accelerated ageing tests are recommended to rigorously validate these extrapolations. Table 5 presents the instantaneous strain at 25 s for each material, together with the predicted creep strain at 10, 20 and 100 years (excluding the instantaneous deformation). For example, the linear extrapolation of TPU suggests a total strain of 0.471 after 20 years, which is consistent with the long-term creep predictions reported previously by Reyes et al. (Reyes et al., 2024). It is evident that creep develops primarily during the early stage of the response, and the creep strain rate decreases markedly after the 10 years. In addition, the

Table 5
Instantaneous strain at 25 s and predicted creep strain of different specimens at 10, 20, and 100 years.

Material	Instantaneous strain (25 s)	Predicted Creep Strain at Time (Years)		
		10	20	100
TPU	0.342	0.124	0.129	0.139
Neoprene	0.531	0.087	0.089	0.094
Neoprene / NBR	0.462	0.124	0.127	0.135
UHMWPE	0.020	0.037	0.038	0.042
PP	0.038	0.026	0.027	0.029
HDPE	0.014	0.029	0.030	0.033

long-term creep predictions for the semi-crystalline polymers are approximately an order of magnitude lower than those of the amorphous polymers, indicating their better creep resistance and their greater suitability for long-term service conditions.

4.7. *Summarising comparison of key characteristics*

For the application of the IRD components investigated in this study within self-centring bridge pier systems, the primary considerations concern two key performance attributes, namely residual deformation and energy dissipation capacity. Under seismic loading, any permanent deformation of the material is directly translated into residual displacement of the pier. It is therefore essential to minimise permanent deformation so that the structure can recover to a state close to its original position following an earthquake. In addition, providing sufficient energy dissipation capacity can markedly enhance the seismic resistance of the bridge, facilitating its use in regions of high seismicity. Other properties are also important. For instance, stress relaxation and stress retention are critical because the energy-dissipating components in segmental piers are typically subjected to sustained prestress. Significant relaxation would reduce their recentering capacity. Furthermore, stiffness, strain hardening and fatigue durability are influential to the long-term performance of the material.

Fig. 23 presents a qualitative comparison of the key characteristics of the six candidate polymer materials. As discussed below, the comparative assessment indicates that TPU is the most suitable candidate, owing to its excellent balance between energy dissipation and self-centring capacity. TPU exhibits very low residual strain and robust energy dissipation even after large cyclic deformations, making it highly appropriate for components required to provide both recentering and long-term energy dissipation. Moreover, TPU shows high stress retention, the lowest stress relaxation, and strong resistance to creep, ensuring that no significant degradation occurs during extended service. UHMWPE exhibits the greatest energy dissipation and a high level of stress retention. However, this is accompanied by substantial permanent deformation, which is detrimental to recentering. For this reason, UHMWPE is not suitable for routine seismic energy-dissipating devices, although it is well suited for replaceable fuse-type elements intended for strong-motion scenarios, where post-event replacement can accommodate its plastic deformation. Neoprene and Neoprene/NBR exhibit low residual deformation and good elasticity, although their relatively low energy dissipation restricts their use. PP provides high compressive strength and considerable energy dissipation, but it shows comparatively low stress retention. HDPE demonstrates high compressive strength and notable energy dissipation, although its relatively low load-bearing capacity and weak strain-hardening response limit its suitability.

5. Conclusions

This study investigated the potential application of six widely used engineering elastomeric materials, TPU, Neoprene, Neoprene/NBR, UHMWPE, Polypropylene, and HDPE, as potential candidates to be used as “intervertebral disc (IRD)” components in damage-free and self-centring spinal bridge piers. Although these materials function solely as compression elements within the proposed structure, a comprehensive investigation into their complex nonlinear mechanical behaviour was conducted by subjecting them to both tensile and compressive

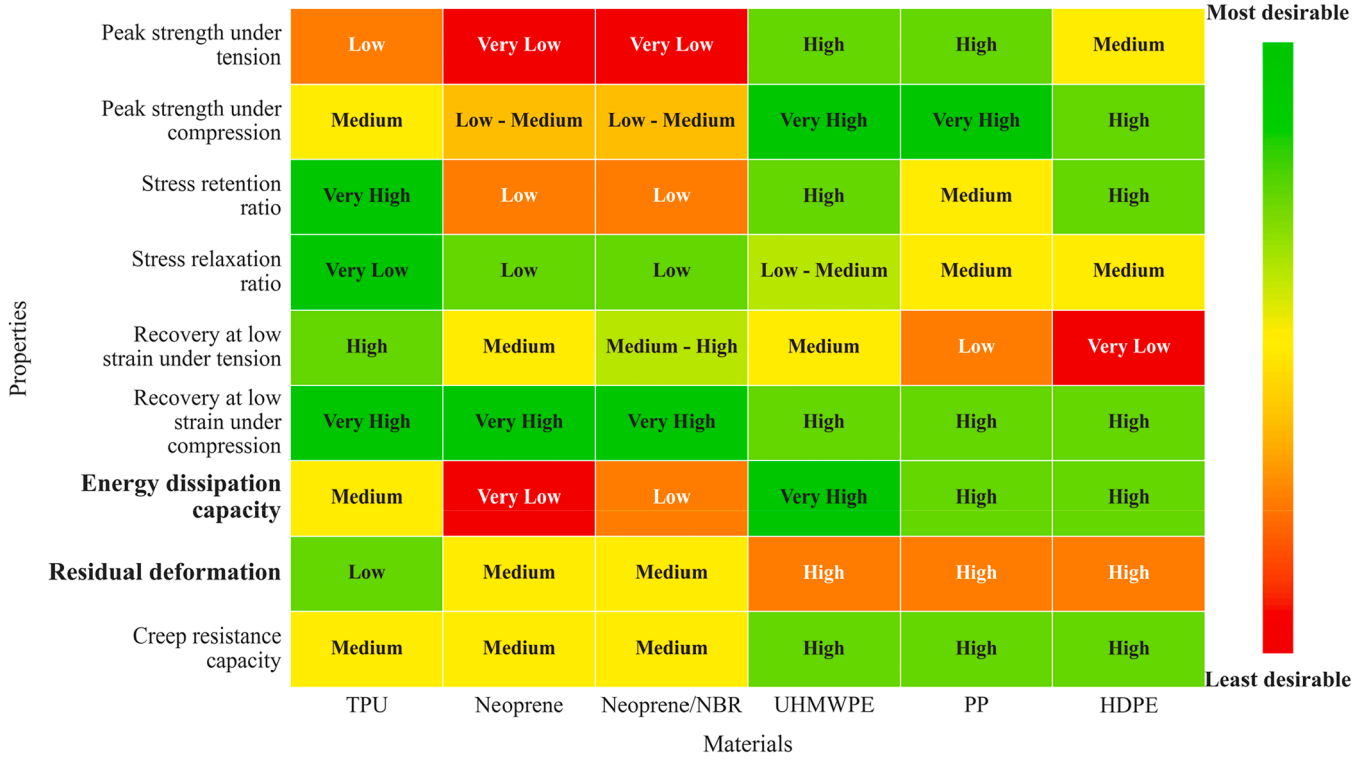

Fig. 23. The comparison of the key characteristics of the six materials.

uniaxial loading protocols. These tests were designed to induce and capture key nonlinear phenomena, including stress softening, stress relaxation, hysteresis, residual strain and recovery, as well as time-dependent creep. The experimental programme successfully captured the distinct behaviours of elastomeric rubbers and thermoplastic polymers under a variety of loading scenarios, thereby providing critical data to support future constitutive model calibration. Overall, the main conclusions are as follows:

1. Cyclic test results indicate that the stress–strain curves of amorphous polymers are close to elastic, with TPU exhibiting a higher elastic modulus, yield-like stress, and the smallest stress relaxation amplitude compared with rubbers. In contrast, semi-crystalline polymers demonstrate a highly nonlinear response, characterised by pronounced yield points, strain-hardening stages, and longer stabilisation in relaxation, with UHMWPE and HDPE showing superior stress retention.
2. Tensile test results reveal that residual strain mainly occurs during the first loading cycle, with no significant additional residual deformation observed in subsequent cycles at the same strain level. Point tracking further shows that, under high strains, HDPE and PP fail through necking and fatigue fracture, respectively, whereas rubbers display better tensile elongation capacity at low strain rates.
3. Under small-strain compressive loading (10 % strain), amorphous polymers almost fully recovered their original shape within 30 min. TPU showed the least residual strain and the highest recovery rate. Semi-crystalline polymers, on the other hand, were limited by irreversible plastic deformation. Furthermore, a fundamental distinction in mechanical response was observed between tension and compression. For instance, HDPE exhibited only 7 % recovery under tensile loading, in contrast to its higher recovery in compression, indicating strong strain-path dependency in semi-crystalline polymers.
4. Large strain compression cycles reveal the energy dissipation capacity of elastomeric materials under extreme seismic loading. UHMWPE demonstrates nearly ten times the energy dissipation of rubbers, with other semi-crystalline polymers slightly lower, though all accompanied by severe permanent plastic deformation. Amorphous polymers dissipate less total energy, but most of their residual deformation is recoverable.
5. Based on the cyclic test results, UHMWPE maintains a maximum instantaneous stiffness modulus of approximately 700 MPa, independent of the applied strain, whereas TPU exhibits an exponential increase in stiffness with strain, rising slowly at first and then rapidly at higher strains. The backbone curves indicate that stiffness evolution does not significantly change with the degradation of energy dissipation.
6. Creep testing revealed the time-dependent behaviour of each material. The majority of creep deformation occurs during the early response (within the first ten years). In addition, the long-term creep predictions for the semi-crystalline polymers are approximately one order of magnitude lower than those of the amorphous polymers, indicating their superior resistance to creep and better suitability for long-term service.
7. In summary, this research demonstrates that TPU exhibited the most favourable combination of high stress retention, low residual strain, and creep resistance, making it a promising candidate for IRD components in self-centring bridge piers, while the generated dataset offers valuable input for future modelling and design optimisation. However, UHMWPE could also be an appropriate candidate, as it benefits from strain hardening and enhanced energy dissipation, while its larger permanent deformation can be replaced after an earthquake, thereby enhancing the seismic performance of the pier under major events.

CRediT authorship contribution statement

Evangelia Georgantzia: Writing – review & editing, Supervision, Methodology, Conceptualization. **Mohammad M. Kashani:** Writing – review & editing, Supervision, Resources, Project administration, Methodology, Funding acquisition, Conceptualization. **Hossein A. Beigi:** Writing – review & editing, Formal analysis, Conceptualization. **Hailong Cao:** Writing – original draft, Software, Investigation, Formal analysis, Data curation. **Karl Minta:** Methodology, Investigation, Formal analysis, Data curation.

Declaration of Competing Interest

The authors declare that they have no known competing financial interests or personal relationships that could have appeared to influence the work reported in this paper.

Acknowledgements

This work was supported by a Marie Skłodowska-Curie Postdoctoral Fellowship under the UKRI Horizon Europe Guarantee Scheme (Project Reference: EP/Z000998/), awarded to the third author (Hossein Agha Beigi). The views and conclusions expressed in this paper are those of the authors and do not necessarily reflect those of the funding bodies.

Data availability

Data will be made available on request.

References

[1] E. Afsar Dizaj, M.R. Salami, M.M. Kashani, Seismic vulnerability analysis of irregular multi-span concrete bridges with different corrosion damage scenarios, Soil Dyn. Earthq. Eng. 165 (2023) 107678, https://doi.org/10.1016/j.soildyn.2022.107678.
[2] M.M. Kashani, H. Moodley, H.O. Aminulai, S. Afshan, D. Crump, Experimental Investigation of Nonlinear Cyclic Behavior of Circular Concrete Bridge Piers with Pitting Corrosion, J. Bridge Eng. 29 (2024) 04024048, https://doi.org/10.1061/JBENF2.BEENG-6482.
[3] M.M. Kashani, J. Maddocks, E.A. Dizaj, Residual Capacity of Corroded Reinforced Concrete Bridge Components: State-of-the-Art Review, J. Bridge Eng. 24 (2019) 03119001, https://doi.org/10.1061/(ASCE)BE.1943-5592.0001429.
[4] Z. Zhang, H.O. Aminulai, W. Powrie, M.M. Kashani, Numerical investigation of the impact of nonuniform corrosion on dynamic characteristics and nonlinear cyclic behaviour of circular RC bridge piers, Bull. Earthq. Eng. 23 (2025) 2233–2264, https://doi.org/10.1007/s10518-025-02131-y.
[5] Chapter 3 Seismic actions ., Emerald Publishing Limited Des. Guide EN 1998-1 1998-5 Eurocode 8 Des. Provis. Earthq. Resist. Struct2005, 0M.FardisE.CarvalhoA.ElnashaiE.FaccioliP.PintoA.PlumierH.GulvanessianM.FardisE.CarvalhoA.ElnashaiE.FaccioliP.PintoA.PlumierH.Gulvanessian10.1680/dgte8.33481.0003.
[6] J. Moehle, State of Research on Seismic Retrofit of Concrete Building Structures in the US, in: 2001. ⟨https://www.semanticscholar.org/paper/State-of-Research-on-Seismic-Retrofit-of-Concrete-Moehle/97827070df652872e43af9aacdabd98a3e6b07ce⟩ (accessed August 11, 2025).
[7] T. Paulay, M.J.N. Priestly. Seismic Design of Reinforced Concrete and Masonry Buildings, 1st ed., Wiley, 1992 https://doi.org/10.1002/9780470172841.
[8] M.J.N. Priestley, F. Seible, G.M. Calvi. Seismic Design and Retrofit of Bridges, 1st ed., Wiley, 1996 https://doi.org/10.1002/9780470172858.
[9] C. Unanwa, Caltrans Seismic Design Criteria 2.1, (n.d.).
[10] A. Wang, LRFD Seismic Bridge Design Published by the American Association of State Highway and Transportation Officials, (n.d.). ⟨https://www.academia.edu/40063133/LRFD_Seismic_Bridge_Design_Published_by_the_American_Association_of_State_Highway_and_Transportation_Officials⟩ (accessed August 11, 2025).
[11] K. Kawashima, G.A. MacRae, J. Hoshikuma, K. Nagaya, Residual Displacement Response Spectrum, J. Struct. Eng. 124 (1998) 523–530, https://doi.org/10.1061/(ASCE)0733-9445(1998)124:5(523).
[12] E. Ahmadi, M.M. Kashani, Seismic vulnerability assessment of precast post-tensioned segmental bridge piers subject to far-fault ground motions, Structures 34 (2021) 2566–2579, https://doi.org/10.1016/j.istruc.2021.09.041.
[13] E. Ahmadi, M.M. Kashani, Numerical investigation of nonlinear static and dynamic behaviour of self-centring rocking segmental bridge piers, Soil Dyn. Earthq. Eng. 128 (2020) 105876, https://doi.org/10.1016/j.soildyn.2019.105876.
[14] Z.-K. Cai, Z. Wang, T.Y. Yang, Cyclic Load Tests on Precast Segmental Bridge Columns with Both Steel and Basalt FRP Reinforcement, J. Compos. Constr. 23 (2019) 04019014, https://doi.org/10.1061/(ASCE)CC.1943-5614.0000944.

[15] C.-C. Chou, Y.-C. Chen, Cyclic tests of post-tensioned precast CFT segmental bridge columns with unbonded strands, Earthq. Eng. Struct. Dyn. 35 (2006) 159–175, https://doi.org/10.1002/eqe.512.
[16] J.T. Hewes, M.J.N. Priestley, Seismic design and performance of precast concrete segmental bridge columns, Dept. of Structural Engineering, University of California, San Diego, La Jolla, Calif, 2002.
[17] W.-P. Kwan, S.L. Billington, Unbonded posttensioned concrete bridge piers. II: Seismic analyses, J. Bridge Eng. 8 (2003) 102–111, https://doi.org/10.1061/(ASCE)1084-0702(2003)8:2(102).
[18] E. Nikbakht, Khalim Rashid, Farzad Hejazi, S.A. Osman, Application of shape memory alloy bars in self-centring precast segmental columns as seismic resistance, Struct. Infrastruct. Eng. 11 (2015) 297–309, https://doi.org/10.1080/15732479.2013.876056.
[19] M.T. Nikoukalam, P. Sideris, Resilient Bridge Rocking Columns with Polyurethane Damage-Resistant End Segments and Replaceable Energy-Dissipating Links, J. Bridge Eng. 22 (2017) 04017064, https://doi.org/10.1061/(ASCE)BE.1943-5592.0001069.
[20] Y.-C. Ou, M.-S. Tsai, K.-C. Chang, G.C. Lee, Cyclic behavior of precast segmental concrete bridge columns with high performance or conventional steel reinforcing bars as energy dissipation bars, Earthq. Eng. Struct. Dyn. 39 (2010) 1181–1198, https://doi.org/10.1002/eqe.986.
[21] Y.-C. Ou, M. Chiewanichakorn, A.J. Aref, G.C. Lee, Seismic Performance of Segmental Precast Unbonded Posttensioned Concrete Bridge Columns, J. Struct. Eng. 133 (2007) 1636–1647, https://doi.org/10.1061/(ASCE)0733-9445(2007)133:11(1636).
[22] P. Sideris, A.J. Aref, A. Filiatrault, Quasi-Static Cyclic Testing of a Large-Scale Hybrid Sliding-Rocking Segmental Column with Slip-Dominant Joints, J. Bridge Eng. 19 (2014) 04014036, https://doi.org/10.1061/(ASCE)BE.1943-5592.0000605.
[23] M.M. Kashani, E. Ahmadi, A. Gonzalez-Buelga, D. Zhang, F. Scarpa, Layered composite entangled wire materials blocks as pre-tensioned vertebral rocking columns, Compos. Struct. 214 (2019) 153–163, https://doi.org/10.1016/j.compstruct.2019.02.021.
[24] M.M. Kashani, A. Gonzalez-Buelga, R.P. Thayalan, A.R. Thomas, N.A. Alexander, Experimental investigation of a novel class of self-centring spinal rocking column, J. Sound Vib. 437 (2018) 308–324, https://doi.org/10.1016/j.jsv.2018.08.034.
[25] M.M. Kashani, A. Gonzalez-Buelga, Nonlinear dynamics of self-centring segmental composite rocking column, Procedia Eng. 199 (2017) 441–446, https://doi.org/10.1016/j.proeng.2017.09.176.
[26] H. Alkarrani, G. ALMisned, H.O. Tekin, A benchmarking analysis on different rubber materials: towards customisation of lightweight and effective radiation protection solutions for aerospace and electronic applications, J. Rubber Res. 28 (2025) 129–141, https://doi.org/10.1007/s42464-024-00272-4.
[27] T. Lei, Y.-W. Zhang, D.-L. Kuang, Y.-R. Yang, Preparation and properties of rubber blends for high-damping-isolation bearings, Polymers 11 (2019) 1374, https://doi.org/10.3390/polym11081374.
[28] Z. Zhang, M.F. Vassiliou, Y. Zhou, S.I. Reyes, D. Konstantinidis, Experimental and numerical studies on thick rubber bearings under uniaxial and offset tensile loading, J. Struct. Eng. 150 (2024) 04024070, https://doi.org/10.1061/JSENDH.STENG-12779.
[29] A.A. Katsamakas, M.F. Vassiliou, Experimental parametric study and phenomenological modeling of a deformable rolling seismic isolator, J. Earthq. Eng. 27 (2023) 4664–4693, https://doi.org/10.1080/13632469.2023.2189978.
[30] S.I. Reyes, E.L. Lopez, M.F. Vassiliou, Validation of a three-dimensional finite element constitutive modeling approach for a thermoplastic polyurethane calibrated with uniaxial tests, Eng. Struct. 322 (2025) 119044, https://doi.org/10.1016/j.engstruct.2024.119044.
[31] A. Rahimi, J.M. García, Chemical recycling of waste plastics for new materials production, Nat. Rev. Chem. 1 (2017) 0046, https://doi.org/10.1038/s41570-017-0046.
[32] A.S. Argon, Cambridge. The Physics of Deformation and Fracture of Polymers, Cambridge University Press, 2013, https://doi.org/10.1017/CBO9781139033046.
[33] 1997, R.N.HawardR.J.YoungThe Physics of Glassy PolymersSpringer NetherlandsDordrecht10.1007/978-94-011-5850-3.
[34] E.M. Arruda, M.C. Boyce, A three-dimensional constitutive model for the large stretch behavior of rubber elastic materials, J. Mech. Phys. Solids 41 (1993) 389–412, https://doi.org/10.1016/0022-5096(93)90013-6.
[35] J.S. Bergström, M.C. Boyce, Large strain time-dependent behavior of filled elastomers, Mech. Mater. 32 (2000) 627–644, https://doi.org/10.1016/S0167-6636(00)00028-4.
[36] Y. Merckel, J. Diani, M. Brieu, J. Caillard, Constitutive modeling of the anisotropic behavior of Mullins softened filled rubbers, Mech. Mater. 57 (2013) 30–41, https://doi.org/10.1016/j.mechmat.2012.10.010.
[37] H.J. Qi, M.C. Boyce, Stress–strain behavior of thermoplastic polyurethanes, Mech. Mater. 37 (2005) 817–839, https://doi.org/10.1016/j.mechmat.2004.08.001.
[38] S.R. Rickaby, N.H. Scott, A cyclic stress softening model for the Mullins effect, Int. J. Solids Struct. 50 (2013) 111–120, https://doi.org/10.1016/j.ijsolstr.2012.09.006.
[39] M.C. Boyce, K. Kear, S. Socrate, K. Shaw, Deformation of thermoplastic vulcanizates, J. Mech. Phys. Solids 49 (2001) 1073–1098, https://doi.org/10.1016/S0022-5096(00)00066-1.
[40] Z. Qi, N. Hu, G. Li, D. Zeng, X. Su, Constitutive modeling for the elastic-viscoplastic behavior of high density polyethylene under cyclic loading, Int. J. Plast. 113 (2019) 125–144, https://doi.org/10.1016/j.ijplas.2018.09.010.
[41] M. Shahzad, A. Kamran, M.Z. Siddiqui, M. Farhan, Mechanical Characterization and FE Modelling of a Hyperelastic Material, Mater. Res. 18 (2015) 918–924, https://doi.org/10.1590/1516-1439.320414.
[42] M.H.R. Ghoreishy, F. Abbassi Sourki, Development of a new combined numerical/experimental approach for the modeling of the nonlinear hyper-viscoelastic behavior of highly carbon black filled rubber compound, Polym. Test. 70 (2018) 135–143, https://doi.org/10.1016/j.polymertesting.2018.06.035.
[43] A.B. Habieb, G. Milani, V. Quaglini, F. Milani, Relaxation test and numerical modeling of rubber for seismic base isolation, AIP Conf. Proc. 2186 (2019) 100011, https://doi.org/10.1063/1.5138017.
[44] S.I. Reyes, M.F. Vassiliou, D. Konstantinidis, Experimental characterization and constitutive modeling of thermoplastic polyurethane under complex uniaxial loading, J. Mech. Phys. Solids 186 (2024) 105582, https://doi.org/10.1016/j.jmps.2024.105582.
[45] M. Hosseini-Farid, M. Ramzanpour, J. McLean, M. Ziejewski, G. Karami, Rate-dependent constitutive modeling of brain tissue, Biomech. Model. Mechanobiol. 19 (2020) 621–632, https://doi.org/10.1007/s10237-019-01236-z.
[46] Y. Xu, D. Li, S. Zhou, Z. Shen, Y. Li, A Rate-Dependent Constitutive Model of HTPB Propellant Based on Parallel Rheological Framework, Propellants Explos. Pyrotech. 47 (2022) e202100334, https://doi.org/10.1002/prep.202100334.
[47] Rubber, vulcanized or thermoplastic. Determination of tensile stress-strain properties Definitive2024.
[48] Rubber, vulcanized or thermoplastic. Determination of compression stress-strain properties Confirmed2017.
[49] C. Casavola, L. Del Core, V. Moramarco, G. Pappalettera, M. Patronelli, Experimental and numerical analysis of the Poisson's ratio on soft polyurethane foams under tensile and cyclic compression load, Mech. Adv. Mater. Struct. 29 (2022) 7172–7188, https://doi.org/10.1080/15376494.2021.1994061.
[50] T.R. Walter, A.W. Richards, G. Subhash, A unified phenomenological model for tensile and compressive response of polymeric foams, J. Eng. Mater. Technol. 131 (2008), https://doi.org/10.1115/1.3026556.
[51] L.R.G. Treloar, Stress-strain data for vulcanised rubber under various types of deformation, Trans. Faraday Soc. 40 (1944) 59–70, https://doi.org/10.1039/TF9444000059.
[52] T. Kida, T. Kimura, A. Eno, K. Janchai, M. Yamaguchi, Y. Otsuki, T. Kimura, T. Mizukawa, T. Murakami, K. Hato, T. Okawa, Effect of Ultra-High-Molecular-Weight Molecular Chains on the Morphology, Crystallization, and Mechanical Properties of Polypropylene, Polymers 13 (2021) 4222, https://doi.org/10.3390/polym13234222.
[53] M. Rendek, A. Lion, Strain induced transient effects of filler reinforced elastomers with respect to the Payne-Effect: experiments and constitutive modelling, ZAMM J. Appl. Math. Mech. Z. F. üR. Angew. Math. Mech. 90 (2010) 436–458, https://doi.org/10.1002/zamm.200900362.
[54] K. Upadhyay, G. Subhash, D. Spearot, Visco-hyperelastic constitutive modeling of strain rate sensitive soft materials, J. Mech. Phys. Solids 135 (2020) 103777, https://doi.org/10.1016/j.jmps.2019.103777.
[55] D.G. Dikobe, A.S. Luyt, Thermal and mechanical properties of PP/HDPE/wood powder and MAPP/HDPE/wood powder polymer blend composites, Thermochim. Acta 654 (2017) 40–50, https://doi.org/10.1016/j.tca.2017.05.002.
[56] X. Zeng, G. Li, J. Zhu, M. Sain, R. Jian, NBR/CR-Based High-Damping Rubber Composites Containing Multiscale Structures for Tailoring Sound Insulation, Macromol. Mater. Eng. 308 (2023) 2200464, https://doi.org/10.1002/mame.202200464.
[57] C. Briody, B. Duignan, S. Jerrams, S. Ronan, Prediction of compressive creep behaviour in flexible polyurethane foam over long time scales and at elevated temperatures, Polym. Test. 31 (2012) 1019–1025, https://doi.org/10.1016/j.polymertesting.2012.07.006.
[58] H. He, Q. Zhang, Y. Zhang, J. Chen, L. Zhang, F. Li, A comparative study of 85 hyperelastic constitutive models for both unfilled rubber and highly filled rubber nanocomposite material, Nano Mater. Sci. 4 (2022) 64–82, https://doi.org/10.1016/j.nanoms.2021.07.003.
[59] M. Amjadi, A. Fatemi, Creep behavior and modeling of high-density polyethylene (HDPE), Polym. Test. 94 (2021) 107031, https://doi.org/10.1016/j.polymertesting.2020.107031.
[60] Y. Otsuki, K. Hashimoto, Y. Kobayashi, S. Nishitsuji, H. Matsuno, H. Ito, Analyzing the tensile creep behavior of different types of polypropylenes using a simple fractional differential viscoelastic model, Polymers 17 (2025) 1095, https://doi.org/10.3390/polym17081095.